Free Radical Biology and Medicine 204 (2023) 252–265

Contents lists available at ScienceDirect

Free Radical Biology and Medicine

journal homepage: www.elsevier.com/locate/freeradbiomed

Performance benchmarking microplate-immunoassays for quantifying target-specific cysteine oxidation reveals their potential for understanding redox-regulation and oxidative stress

Ahmet Tuncay [a,1], Daniel R. Crabtree [a,1], David J. Muggeridge [b], Holger Husi [a], James N. Cobley [a,c,*]

[a] Division of Biomedical Science, Life Science Innovation Centre, University of the Highlands and Islands, Inverness, IV2 5NA, Scotland, UK
[b] Edinburgh Napier University, Edinburgh, Scotland, UK
[c] Cysteine Redox Technology Group, Life Science Innovation Centre, University of the Highlands and Islands, Inverness, IV2 5NA, Scotland, UK

ARTICLE INFO

Keywords:
Cysteine
ALISA
Redox regulation
Oxidative stress
Immunology
Development
Exercise

ABSTRACT

The antibody-linked oxi-state assay (ALISA) for quantifying target-specific cysteine oxidation can benefit specialist and non-specialist users. Specialists can benefit from time-efficient analysis and high-throughput target and/or sample n-plex capacities. The simple and accessible "off-the-shelf" nature of ALISA brings the benefits of oxidative damage assays to non-specialists studying redox-regulation. Until performance benchmarking establishes confidence in the "unseen" microplate results, ALISA is unlikely to be widely adopted. Here, we implemented pre-set pass/fail criteria to benchmark ALISA by robustly evaluating immunoassay performance in diverse biological contexts. ELISA-mode ALISA assays were accurate, reliable, and sensitive. For example, the average inter-assay CV for detecting 20%- and 40%-oxidised PRDX2 or GAPDH standards was 4.6% (range: 3.6–7.4%). ALISA displayed target-specificity. Immunodepleting the target decreased the signal by ~75%. Single-antibody formatted ALISA failed to quantify the matrix-facing alpha subunit of the mitochondrial ATP synthase. However, RedoxiFluor quantified the alpha subunit displaying exceptional performance in the single-antibody format. ALISA discovered that (1) monocyte-to-macrophage differentiation amplified PRDX2-specific cysteine oxidation in THP-1 cells and (2) exercise increased GAPDH-specific cysteine oxidation in human erythrocytes. The "unseen" microplate data were "seen-to-be-believed" via orthogonal visually displayed immunoassays like the dimer method. Finally, we established target ($n = 3$) and sample ($n = 100$) n-plex capacities in ~4 h with 50–70 min hands-on time. Our work showcases the potential of ALISA to advance our understanding of redox-regulation and oxidative stress.

1. Introduction

Technological advances have illuminated redox-regulation [1], the process by which chemically defined sulfur redox state changes post-translationally control proteins [2–4]. For example, many enzyme reactions, such as protein tyrosine dephosphorylation, require the nucleophilic deprotonated sulfur atom [5]. They can be inhibited by oxidising the deprotonated sulfur atom to the soft sulfenic acid electrophile [6]. Technology empowers cysteine discovery science. For instance, the Chouchani group's pioneering mass spectrometric (m/s) cysteine-reactive-phosphate tag technology led to breakthrough discoveries about how ageing affects tissue-specific protein cysteine oxidation [7]. Here, we define the analytical performance benchmarks new microplate-based technologies must meet to advance our understanding of redox-regulation.

The antibody-linked oxi-state assay (ALISA) [8] microplate technology for quantifying target-specific cysteine oxidation can benefit specialists and non-specialists alike.

- **Specialists** can benefit from the "screen" function. Rapidly quantifying cysteine oxidation in a high-throughput manner, such as 96 sample-plex, may be instrumental for selecting a target for follow-up

* Corresponding author. Division of Biomedical Science, Life Science Innovation Centre, University of the Highlands and Islands, Inverness, IV2 5NA, Scotland, UK.
E-mail address: james.cobley@uhi.ac.uk (J.N. Cobley).
[1] Joint-first—the two authors contributed equally.

https://doi.org/10.1016/j.freeradbiomed.2023.05.006
Received 2 April 2023; Received in revised form 24 April 2023; Accepted 5 May 2023
Available online 14 May 2023

m/s analysis. For example, one could analyse a biological pathway to identify stimulus responsive proteins (e.g., lipopolysaccharide-stimulated toll-like receptor signalling pathways). The potential for accurate, reliable, and sensitive performance is useful. For example, sensitivity is essential when the biological material is rate-limiting (e.g., liquid biopsies), especially if the sample is destined for multiple assays. When a protein is redox-regulated, ALISA can quickly discover whether the control mechanism is activated in a new context. For example, ALISA can help translate cell culture insights by quantifying redox-regulated proteins, such as GAPDH, in humans.

- **Non-specialists** can benefit from the ability to quantify target-specific cysteine oxidation using simple, easy-to-implement, and interpret off-the-shelf kits. Indeed, ALISA uses standard lab equipment (e.g., microplate) and well-established techniques (e.g., the ELISA). ALISA brings the benefits of oxidative damage assays (e.g., protein carbonylation or DNA damage ELISA kits) to the study of redox-regulation, which could lead to diverse insights by widening access.

Realising the potential benefits of ALISA relies on robustly evaluating immunoassay performance against established analytical benchmarks. Potential users need to be confident that the "unseen" microplate data truly reflects the target-specific cysteine oxidation state, especially when there are justifiable concerns about the specificity of immunoaffinity reagents [9,10]. They must be validated for the intended application [11]. Establishing analytical benchmarks provides the community with valuable information, such as target-specific reference values. By defining the analytical limits of the technique, performance benchmarking allows the community to rationally use the assay. Guided use is vital for selecting a suitable technique from the rich cysteine oxidation analysis toolbox [12]. The toolbox contains powerful m/s [13] and visually displayed slab-format immunoassay methods [14]. Performance benchmarking exercises that use established tools as gold-standards can showcase how ALISA complements existing technologies. To promote wider use, ALISA must have the potential to empower discovery science in diverse contexts because elementary redox-regulatory mechanisms transcend traditional disciplinary boundaries.

Here, we aimed to performance benchmark ALISA by using pre-set internal, biological, and external pass/fail criteria to determine the utility of the technique in diverse contexts, from development to exercise, and samples, from human cells to tissue. Our work suggests that ALISA, provided key criteria are met, can advance our understanding of redox-regulation across the oxidative eustress/distress spectrum [15–17]. Although we considered oxidative eustress (e.g., exercise), ALISA can study oxidative distress contexts, such as neurodegeneration [18–20]. The results are of value and interest to the many specialists and non-specialists who stand to benefit from ALISA. We consider extending the reach of cysteine oxidation analysis to the microplate format to be of particular significance for high-throughput screens. Proof-of-principle experiments directly demonstrate high-throughput sample ($n = 100$) and target ($n = 3$) n-plex capacities.

2. Results

2.1. Experimental design

To performance benchmark ALISA [8], we used a three-phased approach. Firstly, we set pass/fail criteria to internally benchmark analytical performance across multiple metrics, from accuracy to reliability (see Table 1). The criteria enabled us to identify any potential performance issues. Secondly, we appraised the analytical value of the internally validated microplate-based ALISA assay by determining whether it could generate biological insights. Finally, we externally validated the "unseen" microplate data by comparing it to established visually displayed macroscale immunoassay outputs to determine if the findings were consistent. The macroscale immunoassays included the dimer [21], cysteinyl labelling [22,23], and Click-PEG assays [24–27] as depicted in Fig. 1. Comparative macroscale immunoassay analyses helped to validate the results and provided additional confidence in the performance of ALISA. This approach allowed us to robustly and rigorously performance benchmark ALISA.

Table 1
Type-stratified pre-set pass/fail criteria by performance metric. CV = co-efficient of variation.

Type	Metric	Pass	Fail
Internal	Binding/efficacy	Detects analyte	Analyte undetected
Internal	Accurate	≤5% of the standard redox state	≥6% of the standard redox state
Internal	Reliable	≤10% inter-assay CV ≤5% intra-assay CV	≥11% inter-assay CV ≥6% intra-assay CV
Internal	Specific	Selectivity detects analyte	Unselective—appreciable cross-reactivity
Internal	Sensitive	Detects analyte in ≤3 μg	≥4 μg of sample
Biological	Cysteine oxidation insights	New information is generated	No new information is generated
External	Visual macroscale immunoassay output verification	Agreement—the biological results match	Disagreement—the biological results are mismatched

2.2. Case study 1: PMA-induced monocyte-to-macrophage differentiation amplified PRDX2-specific cysteine oxidation in human THP-1 cells

When it is possible to implement them, many studies use immunoassays to quantify cysteine oxidation in cultured cells. For example, an expanding number quantify peroxiredoxin 2 (PRDX2, UniProt: P32119) using the gold-standard dimer assay [21]. The cysteine-dependent peroxidase, PRDX2 controls antioxidant defence and directs redox signalling in the cytosol by metabolising reactive oxygen species (ROS [28–30]) bearing an O–O bond like hydrogen peroxide [31–34]. The PRDX2 dimer assay enabled us to evaluate the suitability of ALISA as a means to determine the oxidation of the many interesting proteins, such as RAD51 [35], that lack established immunoassays. The ability to do so adds a quick and convenient tool to the cysteine oxidation toolbox. Since cysteine-dependent redox-regulation is emerging as an important control mechanism in immunology [36,37], we performance benchmarked the ability of ALISA to quantify PRDX2-specific cysteine oxidation compared to the gold-standard dimer assay in human-derived THP-1 cells. The extensively used THP-1 cell line (>14,000 PubMed hits) enabled us to quantify PRDX2 oxidation during monocyte-to-macrophage differentiation using an accepted phorbol-12-myristate-13-acetate (PMA) model [38]. Consistent with the utility of the model, established flow cytometry extracellular marker profiling and microscopy analysis confirmed PMA-induced monocyte-to-macrophage differentiation in the THP-1 cells (Supplementary Figs. 1–2).

To perform ALISA, the experimental samples were prepared using validated cysteine-reactive reagents and cysteine-labelling procedures [39]. Cells were lysed with *N*-ethylmaleimide (NEM) buffer to alkylate reduced cysteines via the Michael addition reaction-dependent formation of a thioether bond [40]. Reversibly oxidised cysteines were reduced with 2-Tris (carboxyethyl)phosphine (TCEP) via the nucleophilic phosphine atom and labelled with a maleimide-conjugated fluorescent reporter (F-MAL, fluorescin-5-maleimide) [41,42]. In this format, ALISA detects TCEP-reducible, reversible, cysteine oxidation. Specific analytical strategies are required to measure irreversible

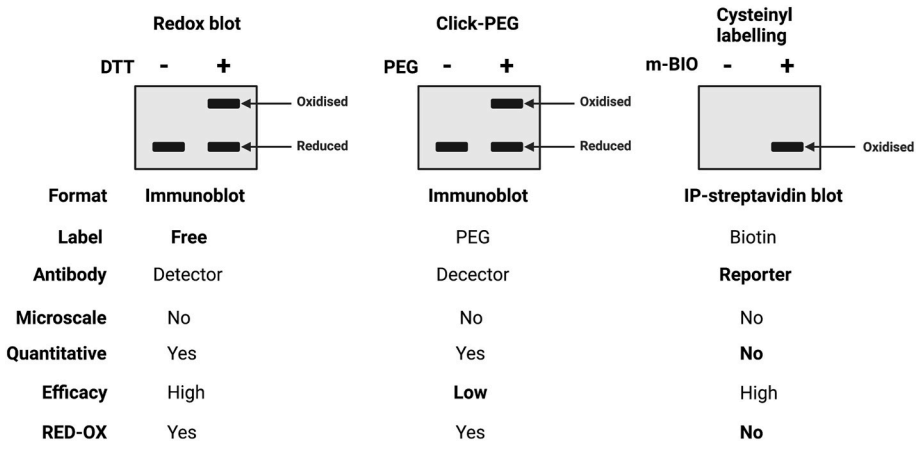

Fig. 1. Scheme of the visually displayed target-specific macroscale immunoassays. From left to right. The redox blot or dimer assay resolves label-free, endogenous, electrophoretic mobility shifts using non-reducing SDS-PAGE. The Click-PEG assay uses ectopic PEG-payloads to induce immunoblot detectable electrophoretic mobility shifts. In the cysteinyl assay, the biotin-conjugated target is captured by IP and reversible cysteine oxidation is detected by streptavidin immunoblotting. None of the assays scale down to the microplate format. Their efficacy is variable. The dimer assay works provided a label-free mobility shift is displayed and the cystineyl labelling assay is extremely effective. In contrast, the efficacy of the Click-PEG assay is low on account of the PEG-payloads blocking antibody binding (see the main text). Unlike the other two assays, the cysteinyl labelling only reports one state (e.g., reversible oxidation). SDS-PAGE = sodium dodecyl sulfate polyacrylamide gel electrophoresis. DTT = 1,4-dithiothreitol.

cysteine oxidation and specific chemotypes. The ELISA-mode ALISA assay uses (1) a capture antibody passively bound to a microplate to "pull-down" PRDX2, and (2) a biotin-conjugated detector antibody to quantify [PRDX2] via streptavidin-conjugated horseradish peroxidase (HRP)-dependent fluorescence (Fig. 2A). PRDX2-specific cysteine oxidation was ratiometrically quantified using equation (1):

$$PRDX2-ox = F - MAL/HRP \quad \text{Equation 1}$$

Internal performance benchmarking confirmed the suitability of the ELISA-mode ALISA assay for the intended application of quantifying PRDX2 cysteine oxidation in THP-1 cells. The assay detected the analyte, as evidenced by a positive HRP signal compared to blank wells (see Supplementary Fig. 3). However, ALISA failed the sensitivity test. We needed >4 μg to detect PRDX2 in THP-1 cells. The insensitivity is a property of the THP-1 cell line used because PRDX2 was detected in <2 μg HeLa cell lysate (see Supplementary Fig. 3). Regarding accuracy and reliability, the assay accurately and reliably determined the cysteine redox state of 20% and 40% standards (see Table 2). Cysteine redox standards are "ground-truth" samples engineered to a set percentage of oxidised protein by mixing 100%-labelled F-MAL and NEM standards as appropriate. For example, 10% oxidised can be created by mixing 1 and 9 parts F-MAL and NEM, respectively. Like most current methods, the labelling is relative, in that, not every cysteine will be labelled in the 100% standard on steric and chemical grounds [40]. All intraassay CV values were below 3%. ALISA displayed target-specificity. Immunodepleting PRDX2 via immunoprecipitation (IP) significantly decreased the F-MAL and HRP signals (see Supplementary Fig. 3).

Table 2
Standard-specific accuracy and reliability data by target for the ELISA-mode ALISA assay. The CV values specify inter-assay variation.

Standard	20%-oxidised				40%-oxidised			
Target	Mean	SD	Diff	CV	Mean	SD	Diff	CV
PRDX2	23	1.0	3.0	3.6	42.3	1.5	2.3	3.6
GAPDH	20.6	1.5	0.6	7.4	41.0	1.6	1.0	3.8

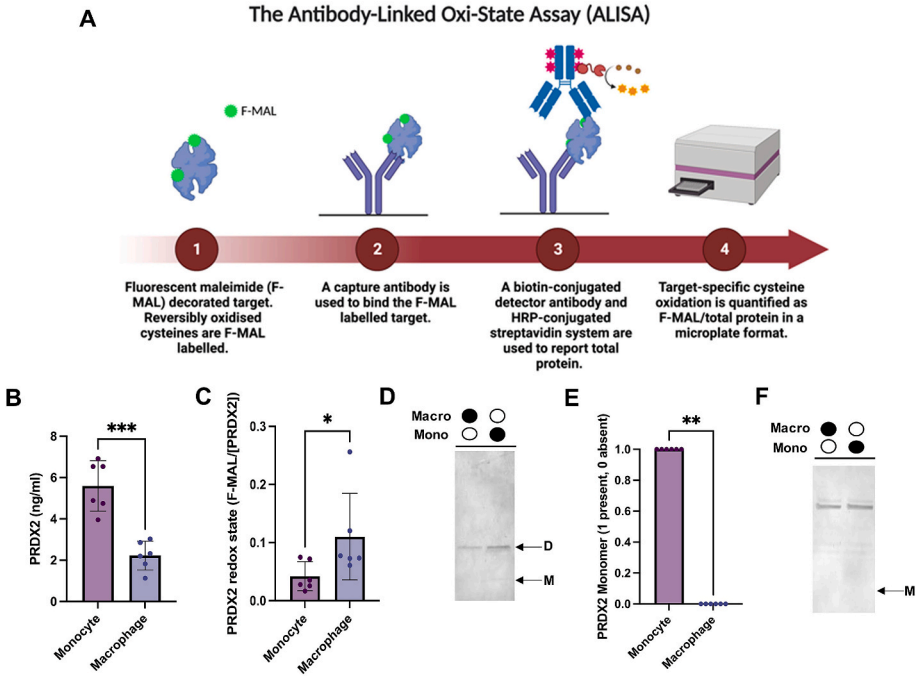

Fig. 2. PMA-induced monocyte-to-macrophage differentiation amplified PRDX2-specific cysteine oxidation in human THP-1 cells. A. Scheme of the ALISA assay. B. PMA-induced monocyte-to-macrophage differentiation ($n = 6$) significantly, as determined by an independent *t*-test, decreased [PRDX2] in THP-1 cells as analysed by the ELISA-mode ALISA assay. C. PMA-induced monocyte-to-macrophage ($n = 6$) differentiation significantly, as determined by an independent Mann-Whitney test, increased PRDX2 oxidation in THP-1 cells as analysed by the ELISA-mode ALISA assay D. Representative PRDX2 dimer assay image. Note the faint monomer band in monocytes (right) and essentially absent band in macrophages (left). E. PMA-induced monocyte-to-macrophage ($n = 6$) differentiation significantly, as determined by an independent Mann-Whitney test, increased PRDX2 oxidation in THP-1 cells as analysed by the dimer assay. The samples were binary scored for the presence (1) or absence (0) of the reduced PRDX2-specific monomeric band. F. Representative anti-PRDX-SO_3 immunoblot image. Note the lack of any monomeric staining. In all panels: ns denotes $P > 0.05$ whereas *, **, ***, and **** denote $P < 0.05$, 0.01, 0.001, and 0.0001, respectively.

Satisfied with the internal performance of the assay, we quantified PRDX2-specific cysteine oxidation following PMA-induced differentiation. ALISA revealed that PMA-induced monocyte-to-macrophage differentiation (1) decreased [PRDX2] by ~50%, from ~5 to 2.4 ng/ml (Fig. 2B), and (2) increased PRDX2-specific cysteine oxidation (Fig. 2C). A benefit of the ALISA assay is that the PRDX2 finding can be contextualised by calculating global proteome wide cysteine oxidation as F-MAL/[protein content], as determined by the BCA assay or equivalent. Interestingly, PMA-induced monocyte-to-macrophage differentiation had no impact on global proteome-wide cysteine oxidation in the THP-1 cells (see Supplementary Fig. 3).

To visually verify the microscale ALISA finding, we used the dimer assay (see Fig. 1) as the gold-standard expert recommended approach for quantifying PRDX2-specific cysteine oxidation [12,21]. The dimer assay quantifies a label-free electrophoretic mobility shift in non-reducing SDS-PAGE induced by an intermolecular disulfide bond covalently stapling two monomers together. In theory, the monomers are reduced (representing 3 reduced cysteines per monomer) and the dimers are oxidised (representing at least two oxidised cysteines per dimer). In practice, the monomers may contain sulfinic acids (RSO_2), sulfonic acids (RSO_3) and/or other oxidised chemotypes (e.g., S-glutathionylated, RSSG) [43]. Likewise, dimers may contain reduced cysteines and other oxidised chemotypes (e.g., RSSG) [44]. In contrast, ALISA, would, for example, label any reversibly oxidised cysteines in the monomers with F-MAL.

Although the differences in what they report could produce a discrepant result, we observed excellent agreement between ALISA and the dimer assay. The dimer assay visually verified the PMA-induced increase in PRDX2-specific cysteine oxidation (Fig. 2D). To our surprise, the monomeric band was absent in the macrophages, which visually confirmed the PMA-induced increase in PRDX2-specific oxidation (Fig. 2E). In monocytes, PRDX2-specific bands were devoid of detectable SO_3 species as evidenced by the lack of a positive band at ~22 kDa (Fig. 2F). Interestingly, reduced monomeric PRDX1 (UniProt: Q06830), the other cytosolic typical 2-Cys isoform, was detected (see Supplementary Fig. 3), which implies selective context-specific PRDX2 oxidation. Even though the protein was substantially oxidised, the ground-truth redox standards demonstrated that reducing PRDX2 with TCEP altered the F-MAL signal (see Table 2 and Supplementary Fig. 3). In summary, ALISA and the dimer assay revealed that PMA-induced monocyte-to-macrophage differentiation amplified PRDX2-specific cysteine oxidation in THP-1 cells. The finding highlights the potential of the ALISA assay to advance understanding of redox-regulation in immune cells and other contexts (e.g., perceiving electromagnetic fields [45]) by quantifying target-specific cysteine oxidation.

2.3. Case study 2: Exercise increased GAPDH-specific cysteine oxidation in human erythrocytes

Translational studies are vital for understanding redox-regulation and oxidative stress, but they almost universally measure oxidative damage [12,21,46–51]. Oxidative damage assays are generally simple and easy-to-use, which makes them accessible to non-specialists. Bringing their benefits to the redox-regulation field would be valuable. It would particularly benefit studies focused on measuring systemic oxidative stress in humans in response to elemental evolutionary-significant stimuli like exercise [52–56]. Exercise can unravel the biological relevance of target-specific cysteine oxidation for inducing beneficial health-promoting adaptations [57–64].

To showcase the benefits of ALISA, we quantified GAPDH-specific (UniProt: P04406) cysteine oxidation before and after a maximal exercise in human erythrocytes [65]. GAPDH is an ideal target because the redox state of the active site cysteine (Cys152) controls glucose metabolism. It provides erythrocytes with a transcription-independent mechanism to rapidly fine-tune their response to physiological stimuli like exercise [66]. Oxidising GAPDH could induce a redox-regulatory response to exercise by enabling the erythrocyte to produce NADPH via channelling glucose into the pentose phosphate pathway [67,68]. Studying GAPDH may help us understand how essential oxygen transporting cells adapt to exercise [69].

Internal validation experiments revealed that ELISA-mode ALISA (1) detected GAPDH (passed) with 1 μg protein input (sensitivity pass) (Fig. 3A and Supplementary Fig. 3); (2) accurately discriminated between the 20 and 40% cysteine redox standards in a reliable way (passed, see Table 2), (3) all intraassay CVs were less than 2% (passed), and (4) immunodepleting GAPDH significantly decreased the F-MAL and HRP signals by 70–90% (passed, Fig. 3B–C).

Satisfied with the internal performance of the assay, we quantified GAPDH-specific cysteine oxidation before and after maximal exercise in erythrocytes from adult human males. Exercise significantly increased GAPDH-specific cysteine oxidation (Fig. 3D) without changing [GAPDH] (Fig. 3E). Consistent with our previous work [65], exercise had no statistically significant impact on global cysteine oxidation in human erythrocytes (Fig. 3F).

Unlike PRDX2, GAPDH fails to display a label-free mobility-shift in non-reducing PAGE [14]. To visually verify the finding, we performed cysteinyl labelling [22,23]. The cysteinyl labelling assay (see Fig. 1) is an important analytical tool widely used by the community [70]. Notable recent insights include helping to discover cysteine redox-switches in CDK2 [71] and Gasdermin D [72]. To implement the technique, one (1) biotin-conjugated maleimide or equivalent labels reversibly oxidised cysteines, (2) enriches the target via IP, and (3) quantifies cysteine oxidation by streptavidin-immunoblotting. Since we had F-MAL labelled lysates, we modified the assay. Specifically, we replaced biotin-maleimide with F-MAL and used the biotin-conjugated detector antibody to quantify the target to avoid interference from capture antibody-derived light and heavy chains. The modified cysteinyl labelling assay confirmed that maximal exercise significantly increased GAPDH-specific cysteine oxidation in human erythrocytes (Fig. 3G–H). In summary, ALISA and the cysteinyl labelling immunoassays revealed that maximal exercise increased GAPDH-specific oxidation in human erythrocytes. ALISA can advance our understanding of redox-regulation and oxidative stress in humans.

2.4. Case study 3: Breaking ALISA: defining the performance limits of the immunoassay

Like any technique, ALISA is ideal for some analytical tasks like high-throughput targeted cysteine oxidation analysis and ill-suited to others [8]. One such task relates to quantifying cysteine oxidation in a single antibody format when no matched-pair ELISA kits are available, as is the case for most proteins [73]. The single antibody format challenges ALISA due to the need to quantify target protein content without a HRP system. To test the analytical capacity of ALISA, we attempted to quantify the cysteine redox state of the alpha subunit (UniProt: P08428) from the mitochondrial ATP synthase in unfertilised *Xenopus laevis* (*X. laevis*) eggs [74]. Technically, no matched pair reagents were available to analyse the alpha subunit in an ELISA format. Biologically, the alpha subunit defined an example of a redox-regulated protein implicated in controlling mitochondrial bioenergetics [75,76]. As recent work shows [77], redox-regulation may be instrumental for suppressing mitochondrial superoxide production to prevent DNA damage during oogenesis [78]. Finally, one of the key anticipated uses of ALISA is to rapidly determine whether cysteine oxidation is relevant in a new biological context by quantifying the ever-expanding list of redox-regulated proteins [7], such as the alpha subunit.

In the single antibody format [8], ALISA involves (1) covalently binding a capture antibody to a microplate like one bearing epoxy groups for strain-promoted nucleophilic substitution reactions with amines [79], (2) pulling-down the F-MAL labelled target, (3) labelling the resultant immunocomplex with AlexaFluor®647-conjugated *N*-hydroxysuccinimide (F–NHS), and (4) denaturing the

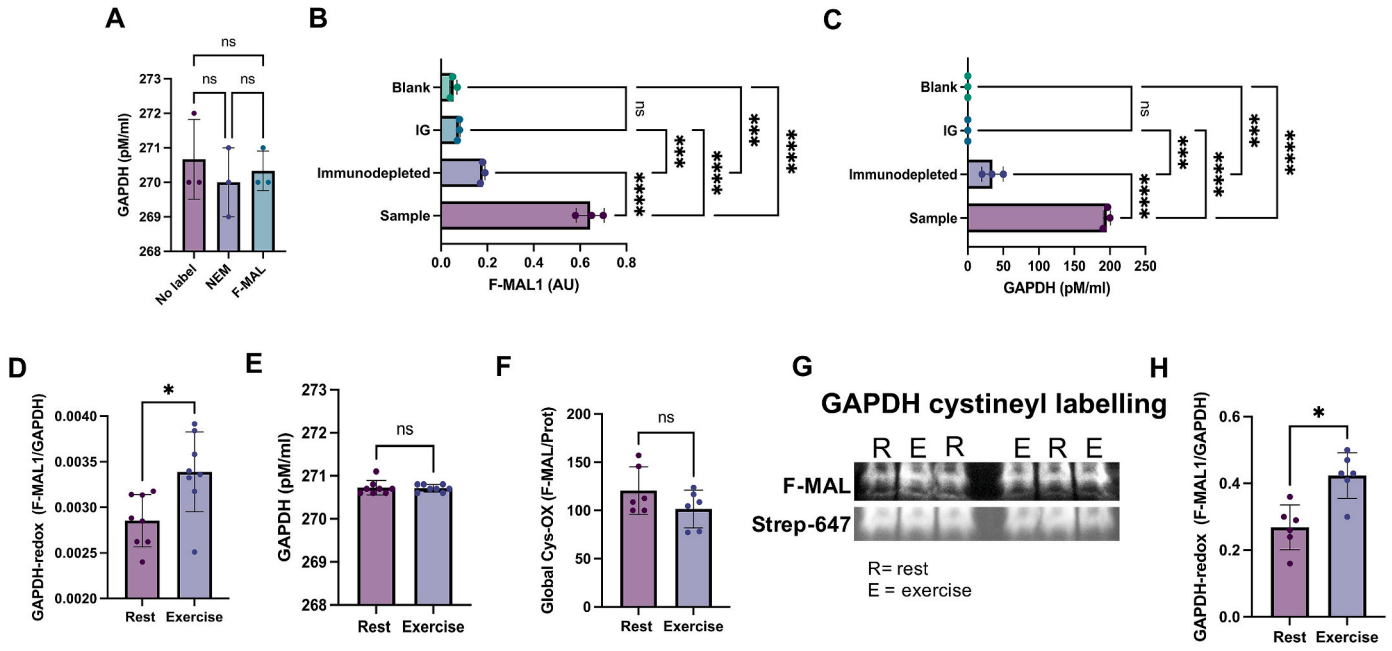

Fig. 3. Exercise increased GAPDH-specific cysteine oxidation in human erythrocytes. A. No impact, as determined by a 1-way ANOVA with Tukey post-hoc testing, of the label on the ability of the ELISA-mode assay to quantify [GAPDH) in human erythrocyte standards ($n = 3$). B–C. Immunodepleting GAPDH significantly as determined by a 1-way ANOVA with Tukey post-hoc testing, decreased the F-MAL (B) and HRP (C) signal in the ELISA-mode ALISA assay. D. Exercise significantly, as determined by an independent *t*-test, increases GAPDH cysteine oxidation, as determined by ELISA-mode ALISA, in human erythrocytes ($n = 8$). E. No significant, as determined by an independent *t*-test, impact of exercise on [GAPDH], as determined by ELISA-mode ALISA, in human erythrocytes ($n = 8$). F. No significant, as determined by an independent *t*-test, impact of exercise on proteome-wide cysteine oxidation, as determined by global-mode ALISA, in human erythrocytes ($n = 8$). G. Representative cysteinyl labelling assay image showing the GAPDH-specific F-MAL (top) and AlexaFluor™647streptavidin signals (bottom) in human erythrocytes before and after exercise. H. Exercise significantly, as determined by an independent *t*-test, increases GAPDH cysteine oxidation, as determined by the cysteinyl labelling assay, in human erythrocytes ($n = 8$). In all panels: ns denotes $P > 0.05$ whereas *, **, ***, and **** denote $P < 0.05$, 0.01, 0.001, and 0.0001, respectively.

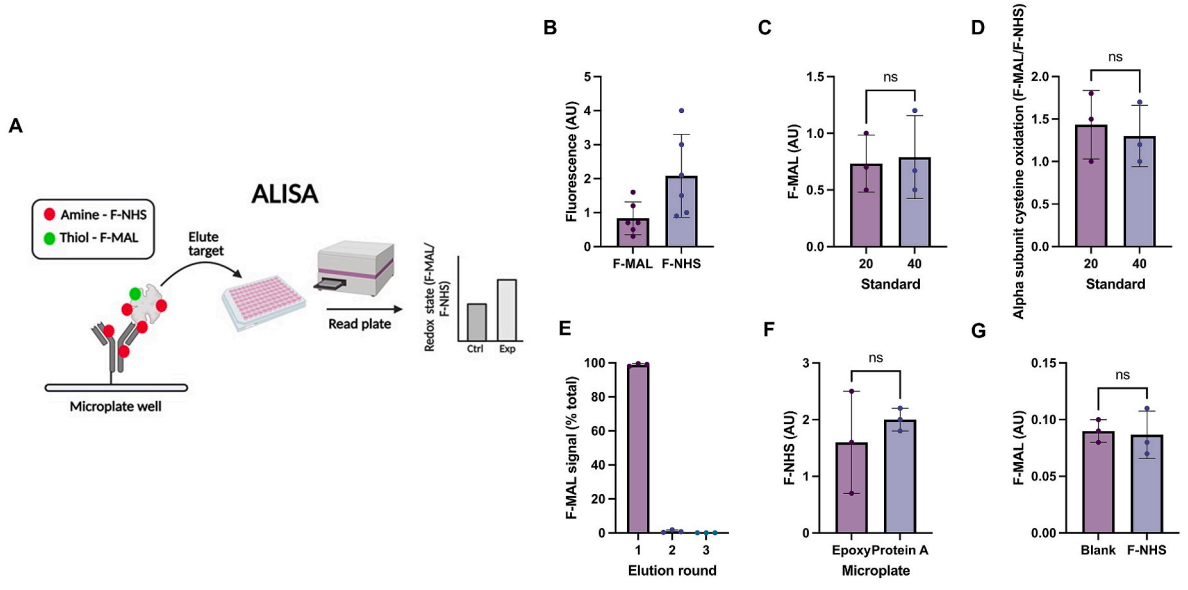

Fig. 4. Breaking ALISA: Defining the performance limits of the immunoassay. A. Schematic overview of the single antibody formatted ALISA assay. B. Erratic fluorescent F-MAL and F–NHS values indicative of an inability to detect the alpha subunit analyte in unfertilised *X. laevis* eggs ($n = 6$). C-D. Inability of the alpha subunit ALISA assay to discriminate, as determined by independent t-tests, between 20 and 40%-oxidised cysteine redox state standards ($n = 3$) derived from unfertilised *X. laevis* eggs. E. Virtually all of the F-MAL signal is eluted in the first round. F. No significant difference, as determined by an independent *t*-test, in the F–NHS signal from the 100%-F-MAL labelled *X. laevis* standards in the epoxy ($n = 3$) compared to protein A mode format ($n = 3$). G. Inability of the protein A mode ALISA assay to detect the alpha subunit in pre-F-NHS labelled *X. laevis* standards indicated by the lack of a statistical difference, as determined by an independent *t*-test, in experimental sample ($n = 3$) treated wells compared to blanks ($n = 3$) in *X. laevis*. In all panels, ns denotes non-significant whereby is $P > 0.05$.

immunocomplex to selectively elute the target from the covalently immobilised capture antibody. The assay quantifies target-specific cysteine oxidation as: F-MAL/F–NHS (Fig. 4A).

Unfortunately, the single antibody format, unilaterally failed to pass the internal performance benchmarking criteria. First, the F-MAL and F–NHS signals for the 100% labelled standard varied substantially: CV value above 58% indicated a detection issue (Fig. 4B). The assay failed to discern between the 20 and 40% cysteine redox state standards (Fig. 4C–D). Inaccurate detection was compounded by erratic performance, with the CV values for the 20 and 40% oxidised standards being above 40%. The performance problems were unrelated to ineffective target elution because the first elution round captured 99% of the F-MAL signal (Fig. 4E).

Mechanistically, some of the unacceptable performance related to randomly covalently bonding the capture antibody to the epoxy microplate paired with variable F–NHS access to target amines. The underpinning evidence comes from experiments comparing the F-MAL and F–NHS signals in the epoxy compared to protein A plates. Correctly orientating the antibody via protein A binding to the Fc domain allowed better F–NHS access, resulting in more uniform (CV for the F–NHS signal = 10%) labelling (Fig. 4F). However, one cannot separate the antibody- and target-dependent F–NHS signals to quantify target-specific cysteine redox state because SDS releases the capture antibody from protein A. Pre-labelling the sample with F–NHS to bypass the antibody-target separation problem introduced another: masking positively charged amine groups seemed to electrostatically impede epitope-paratope binding. Impaired epitope-paratope binding was evidenced by the F-MAL signals from samples incubated with the capture antibody being formally equivalent (statistically no different) from the background (Fig. 4G).

Defining the analytical limits of ALISA may inspire smart chemistry-enabled innovations underpinning next-generation ALISA-v2 assays. Until then, microplate assays must still be able to analyse proteins lacking ELISA reagents, such as the alpha subunit. To meet this pressing analytical need, we used RedoxiFluor [80]. RedoxiFluor uses two spectrally distinct F-MAL labels to quantify target-specific cysteine redox state in relative percentage terms in a protein A coated microplate (see Supplementary Fig. 4). The labels are fluorescein-5-maleimide (F-MAL1, reduced) and AlexaFluor™647-C_2-maleimide (F-MAL2, reversibly oxidised).

Internal validation experiments revealed that (1) RedoxiFluor quantified the alpha subunit with just 0.5 μg input (detection and sensitivity pass, see Supplementary Fig. 4), (2) the F-MAL labels had no impact on antibody recognition, as evidenced by the ability to construct the standard curve (Fig. 5A) and the ability of the capture antibody to bind the PEG-conjugated protein (Fig. 5D), (3) RedoxiFluor accurately and reliably quantified alpha subunit cysteine redox state across the 10–90% oxidised standards curve (see Table 3); and (4) immunodepleting the alpha subunit substantially decreased the F-MAL signal by ~64% (Fig. 5B). The estimated 3.7 μM amount of the alpha subunit per unfertilised *X. laevis* egg [81], presented challenges for immunodepleting it. Some F-MAL signal (~35%) remained because the alpha subunit must be immunodepleted to fM levels to abolish the F-MAL signal when 1–5 pM of capture antibody can bind to the protein A plate. Using the natural knock-out of the erythrocyte lysates devoid of mitochondria completely abolished the F-MAL signal (see Supplementary Fig. 4).

After satisfying assay performance criteria, we quantified alpha subunit-specific cysteine redox state in unfertilised *X. laevis* eggs using

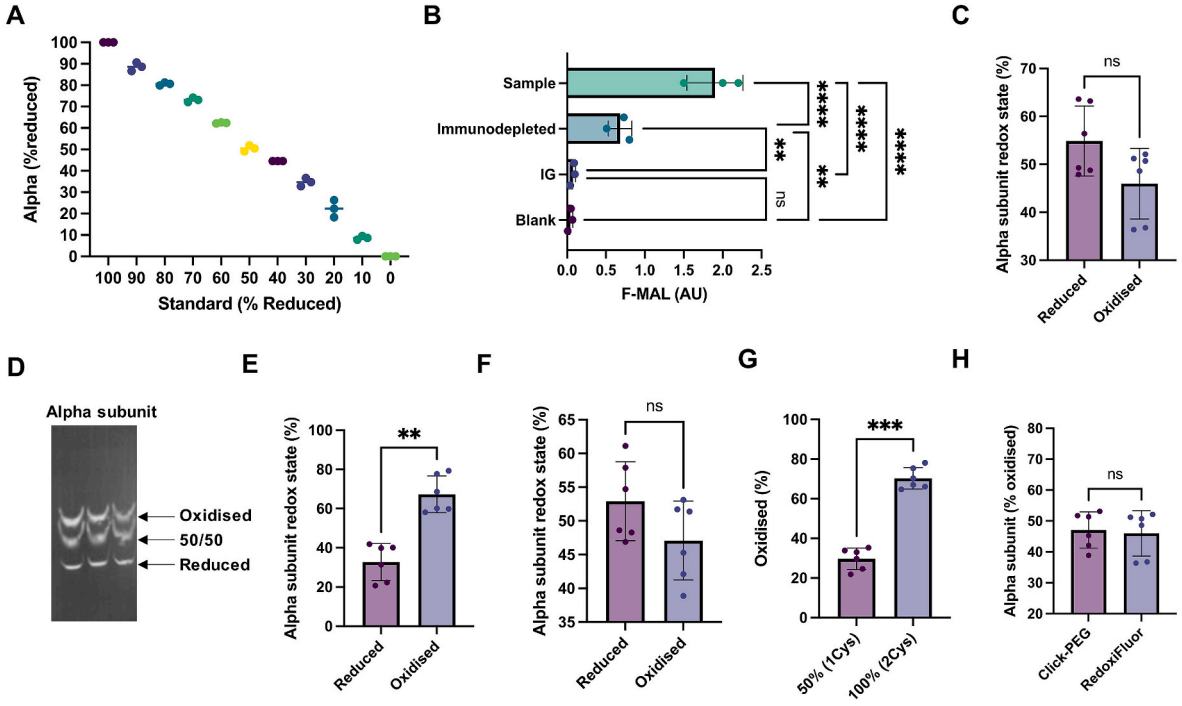

Fig. 5. The alpha subunit of the mitochondrial ATP synthase is oxidised in unfertilised *X. laevis* eggs. A. Excellent relationship between the "ground-truth" cysteine redox state input ($n = 3$) and the protein A-mode RedoxiFluor immunoassay outputs for the alpha subunit in *X. laevis*. B. A significant, as determined by a 1-way ANOVA with post-hoc Tukey testing, decrease in the F-MAL signal output of the alpha subunit RedoxiFluor immunoassay in immunodepleted ($n = 3$) compared to experimental samples ($n = 3$). C. No significant, as determined by a dependent *t*-test, in the redox state of the alpha subunit, as analysed by protein A-mode RedoxiFluor, in unfertilised *X. laevis* eggs ($n = 6$). D. Representative image from the Click-PEG immunoblot assay. E. Without correction for the redox state of the middle band, the alpha subunit is significantly, as determined by a dependent *t*-test, more oxidised than reduced in unfertilised *X. laevis* eggs ($n = 6$). F. When the redox state of the middle band is accounted for, there is no significant, as determined by a dependent *t*-test, in the redox state of the alpha subunit, as analysed by Click-PEG, in unfertilised *X. laevis* eggs ($n = 6$). G. The 100% oxidised form ($n = 6$) is significantly, as determined by a dependent *t*-test, more abundant than the 50% form ($n = 6$). H. No significant difference, as determined by an independent *t*-test, in the alpha subunit oxidation as analysed by Click-PEG ($n = 6$) or RedoxiFluor ($n = 6$). In all panels: ns denotes $P > 0.05$ whereas *, **, ***, and **** denote $P < 0.05$, 0.01, 0.001, and 0.0001, respectively.

Table 3
Cysteine redox state ($n = 3$) performance data for the alpha subunit protein A mode RedoxiFlour assay. The range is the difference between the maximum and minimum value.

Standard % oxidised	Mean (SD)	Difference to ground-truth (%)	Range (%)	Intra-assay CV (%)	Inter-assay CV (%)
90	88.6 (2)	1.4	4	0.5	2.3
80	80.6 (0.7)	0.6	1.4	0.1	0.9
70	73.2 (1.1)	3.2	2.1	0.9	1.4
60	62.4 (0.3)	2.4	0.5	0.1	0.4
50	50.5 (1.5)	0.5	2.9	0.8	2.9
40	44.5 (0)	4.5	0	0.1	0
30	34.7 (1.9)	4.7	3.8	0.2	5.5
20	22.3 (4.0)	2.3	8	1.1	17.9
10	8.7 (0.9)	1.3	1.7	0.7	9.8
Mean	**n/a**	**2.3**	**2.7**	**0.5**	**4.5**

RedoxiFluor. RedoxiFluor revealed that the alpha subunit was 45% oxidised (Fig. 5C). To visually verify RedoxiFluor, we used Click-PEG. Click-PEG deploys catalyst-free inverse electron demand Diels Alder (IEDDA) chemistry [82,83] to ligate reversibly oxidised cysteines with electrophoretic mobility-shifting PEG-payloads (see Fig. 1). Although the PEG-payloads sterically block antibody binding for most targets [14], the approach is feasible for the alpha subunit [27,74]. Click-PEG revealed that the alpha subunit is 65% oxidised in unfertilised *X. laevis* eggs (Fig. 5D–E). The appreciable 20% difference in immunoassay outputs was reconciled. The middle band (+5 kDa) contained 1 reduced and 1 oxidised cysteine (50% oxidised). When the redox state of the middle band was accounted for, the alpha subunit is 47% oxidised (Fig. 5F). Interestingly, the 100% oxidised (2-Cys, +10 kDa) band accounted for more of the oxidised signal compared to the 50% band (Fig. 5G). The 100% oxidised (Cys244 & 294) form accounted for ~25% of the total signal. Despite their disparate methodologies, the percent oxidised alpha subunit values differed by just 2%: 45% in RedoxiFluor compared to 47% oxidised in Click-PEG (Fig. 5H). In summary, ALISA is unsuited to the single antibody format, but RedoxiFluor performed exceptionally well.

2.5. Chemotype-specific ALISA revealed PPP2CA-specific S-glutathionylation in X. laevis

Although it is often beneficial when screening proteins to be agnostic of any one specific type of reversible cysteine oxidation, chemotype-specific approaches are mechanistically important [84,85]. An advantage of ALISA and RedoxiFluor is that they readily can be modified to quantify chemotype-specific oxidation by implementing a reaction- or selective reduction-based strategy [86–88]. To showcase this analytical property, we chemically-induced S-glutathionyation (RSSG) in unfertilised *X. laevis* eggs reduced with TCEP (see methods). To do so, we used xanthine oxidase (UniProt: P47989) to produce superoxide and hydrogen peroxide, per the superoxide dismutase assay [89], so as to form protein sulfenic acids (RSOH). Ectopically applied oxidised glutathione (GSSG) would then convert RSOH to RSSG. To selectively reduce GSSG, we used a mutant glutaredoxin 3 (GRX3) from *E. coli* per previous research [90]. Global-mode ALISA confirmed that the xanthine oxidase system increased reversible cysteine oxidation (Fig. 6A). Increased reversible cysteine oxidation was abolished when copper zinc superoxide dismutase (SOD1, UniProt:P00441) and catalase (CAT, UniProt: P04040) were added (Fig. 6A). Adding GSSG significantly increased reversible cysteine oxidation in a SOD1-CAT dependent manner (Fig. 6B).

Satisfied with the performance of the PSSG-inducing system, we analysed the catalytic subunit of the PP2A serine threonine phosphatase (PPP2CA, UniProt: Q8AVH9) in *X. laevis*. PPP2CA was selected because we have previously validated the ELISA-mode ALISA assay [65] for it and because it is the subject of our on-going work on the redox-regulation of fertilisation. Adding GSSG significantly increased PPP2CA-specific S-glutathionylation without changing PPP2CA protein content in *X. laevis* eggs (Fig. 6C–D). In principle, other strategies for studying reversible and irreversible cysteine oxidation could be implemented [91], most notably the recently developed RSOH reactive turn-on fluorescent probes from the Carroll group [88]. Data demonstrate that ALISA can quantify chemotype-specific cysteine oxidation.

2.6. Proof-of-concept sample and target n-plex capacity examples

The case studies evidenced the advantages and disadvantages of ALISA in relatively small scale (≤10 per group) owing to the need to benchmark it against macroscale immunoassays. Slab-gel formatted macroscale immunoassays are particularly unsuited to high-throughput applications. Inspired by how the Sikes group [92] used a genetically encoded peroxiredoxin-based probe [93] to determine whether 600 compounds induced intracellular hydrogen peroxide, we explored high-throughput ALISA functions. Proof-of-concept experiments tested

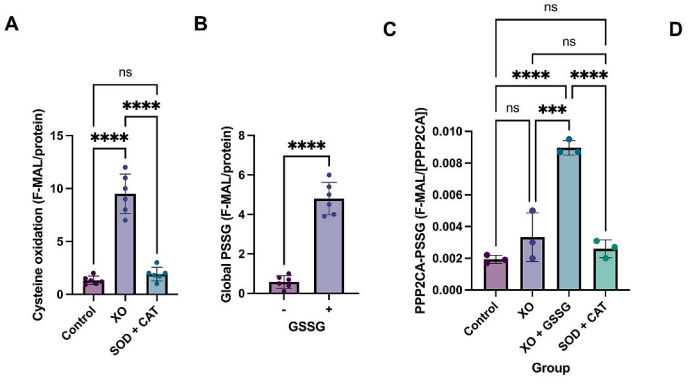

Fig. 6. Chemotype-specific ALISA revealed PPP2CA-specific S-glutathionylation in *X. laevis*. A. Xanthine oxidase (XO) significantly, as determined by a one-way ANOVA test, increased reversible cysteine oxidation, as determined by global mode ALISA, in unfertilised eggs *X. laevis* compared to control (no XO) and antioxidant treated (XO + SOD + CAT) samples ($n = 6$). B. Introducing GSSG (5 mM) into unfertilised *X. laevis* egg lysates treated with XO significantly, as determined by an independent *t*-test, increased protein S-glutathionylation (RSSG), determined using global mode ALISA with a selective RSSG reduction step, compared to control (no GSSG) samples ($n = 6$). C. Chemically-induced PSSG significantly, as determined by a one-way ANOVA, increased PPP2CA-specific S-glutathionylation, as determined using ELISA-mode ALISA with a selective PSSG reduction step, in *X. laevis* ($n = 3$ per group). D. No treatment ($n = 3$ per group) had any significant impact on PPP2CA-content as determined using ELISA-mode ALISA in *X. laevis*. In all panels: ns denotes $P > 0.05$ whereas *, **, ***, and **** denote $P < 0.05$, 0.01, 0.001, and 0.0001, respectively.

target or sample n-plex capabilities. For example, with 96-well and technical duplicates, one could assess 48 targets in 1 sample or 1 target in 48 samples. We determined whether ALISA could quantify GAPDH-specific cysteine oxidation in 100 Hela lysate derived redox standards ($n = 10$ biological replicates in each group from 10 to 100% oxidised, 200 discrete datapoints with technical replicates). In ALISA, redox standards rely on (a) constant [target] and (b) F-MAL signal linearity. After verifying the underlying assumptions about a (amount = ~650 pM/ml) and b (R = 0.97) (Fig. 7A–B), ALISA successfully analysed 100 samples (Fig. 7C). In principle, one can now use ALISA to unmask how a chemical library impacts target-specific cysteine oxidation, which may help unravel their mode-of-action.

Previously, we developed array-mode using RedoxiFluor [80]. Compared to ALISA, RedoxiFluor is better suited to array-mode because it can effectively operate with a single capture antibody. However, we expect that many labs, as confirmed by collaborators [94], wishing to n-plex targets only have NEM or equivalent treated samples. To establish proof-of-principle for the n-target plex capacity, we simultaneously analysed aurora b (UniProt: Q96GD4), CDK6 (UniProt: Q00534), and cdc25c (UniProt: P30307) using ELISA-mode ALISA in Hela lysate derived redox standards. Aside from verifying that immunodepleting the target substantially (−80-90%) decreased the HRP signal (see Supplementary Fig. 4), we omitted performance benchmarking on the basis that the idea of an array is to select a target for follow-up analysis. We analysed duplicate case and controls samples. Aside from the 40%-oxidised cdc25c case "hit" mimic, all the samples were 20%-oxidised. ALISA successfully analysed 8 duplicate samples per group per target (96 discrete datapoints in total) and correctly identified the cdc25c "hit" (Fig. 7D–E). After the overnight binding step, one can run ALISA in ~4 h with 50–70 min actual hands-on time (Fig. 7F). Our results evidence high-throughput ALISA capabilities. Target n-plex can be increased by an order of magnitude provided suitable reagents are available.

3. Discussion

To determine the potential of the ALISA to advance our understanding of redox-regulation, we aimed to evaluate the analytical value of ALISA by performance benchmarking the technique across diverse case studies spanning fundamental processes and explore its potential for high-throughput cysteine oxidation analysis. Key findings are threefold. First, internal validation data confirmed that ALISA is well-suited to analysing PRDX2 (passed) and GAPDH (passed) and ill-suited to quantifying the alpha subunit (failed). The data and the associated metadata define a valuable resource for robustly appraising the suitability of ALISA for the intended application. Defining the analytical limit of the assay, rationally informs a new recommendation: single-antibody format use of ALISA is discouraged. The ELISA-mode ALISA assay performs much better. Second, ALISA generated new biological insights in diverse contexts. PMA-induced monocyte-to-macrophage differentiation amplified PRDX2 oxidation in THP-1 cells and exercise increased GAPDH oxidation in human erythrocytes. The "unseen" microplate discoveries were "seen-to-be-believed" being verified by visually displayed macroscale immunoassays. Third, we demonstrated high-throughput sample or target n-plex ALISA capacities. Our work highlights the pros and cons of using ALISA to advance our understanding of redox-regulation and oxidative stress.

The key strengths of ALISA for quantifying target-specific cysteine oxidation include time-efficient and high-throughput analysis combined with minimal reagent consumption. The 4–5 h workflow duration requires 50–70 min hands-on time to analyse 96-samples using 0.1 μg of capture antibody per sample. In contrast, slab-gel formatted immunoassays require more hands on-time (~2–3 h) and consume far more reagents, such as 1 μg antibody per sample. Compared to the pitfalls of densitometry [95], the microplate format affords rapid (9.6 s per plate), unbiased, and automated analysis. The simple off-the-shelf nature of ALISA widens access by bringing the benefits of widely adopted oxidative damage assays to the study of redox-regulation. Provided suitable reagents are available, ALISA can be applied to diverse biological contexts. When the assay is internally performance benchmarked, we expect the accuracy, reliability, and sensitivity to empower question-driven target-specific discovery science across the oxidative eustress-distress spectrum. As directly demonstrated here by discoveries in immunology, development, and exercise. Interpreting the discovery brings another strength into play. Mechanistically, ALISA outputs integrate

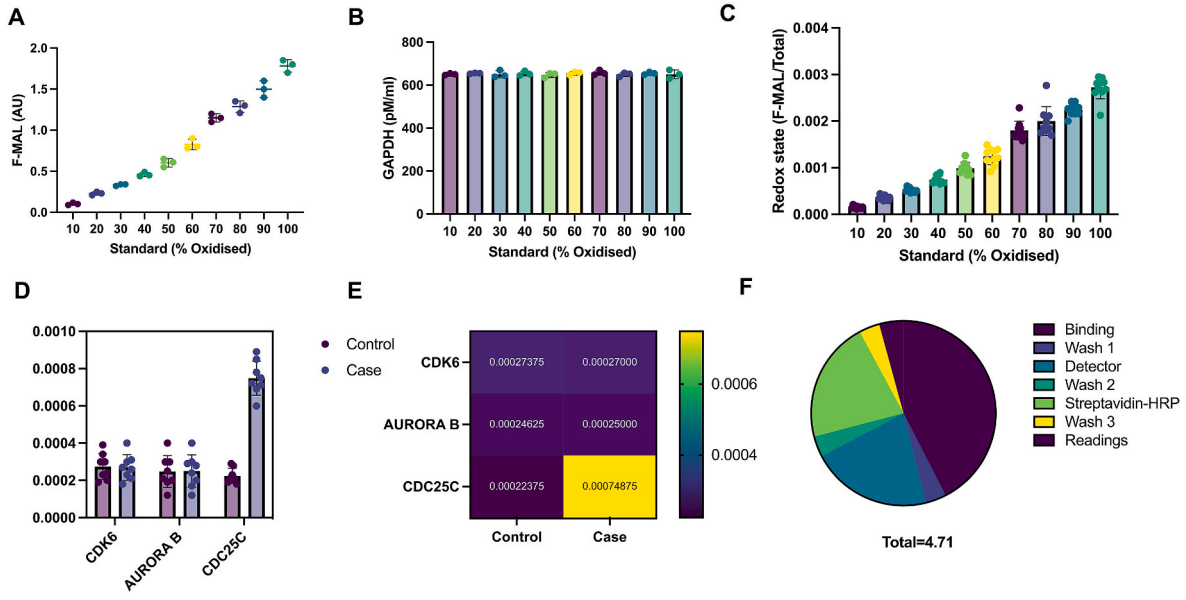

Fig. 7. High-throughput sample and target n-plex capability. A. Linear (R = 0.97) increase in the GAPDH-specific F-MAL1 in the 10–90% cysteine redox state standards ($n = 3$) derived from Hela cells. B. Consistent GAPDH capture amounts across the 10–90% cysteine redox state standards ($n = 3$) derived from Hela cells. C. GAPDH ELISA-mode ALISA 100 sample n-plex data for 10–90% cysteine redox state standards ($n = 10$ per group) derived from Hela cells. D-E. Proof-of-concept 3-target—CDK6, Aurora b, and CDC25c—n-plex data in mock control ($n = 8$) and case ($n = 8$) Hela samples displayed as a bar chart (E) and heatmap (F). The cdc25c "hit" is indicated in yellow (see main text). The 20% or 40%-oxidised cysteine standards derived from Hela cells were used. F. Visual summary of the ALISA workflow time displaying the contribution of each step to the total time.

target-specific cysteine oxidation "on" and reduction "off" chemistry across residues into one holistic metric. The output metric is a redox barometer that dynamically responds to ROS and antioxidant defence. Depending on the protein it can also report function, such as the activation of a biological pathway.

ALISA cannot disclose residue-specific cysteine redox state. Powerful m/s methods remain unmatched in their capacity for n-target plex ($\geq 10^3$ proteins), residue-resolution across $\sim 10^{3-4}$ sites, and sensitivity (single cell analysis is possible [96–98]). Although there are other trade-offs (e.g., the protein inference problem [99–101]), m/s is unconstrained by immunoaffinity reagent availability and their cross-reactivities. The selectivity of the immunoaffinity reagent cannot be assured. Or guaranteed even when a target is validated due to intrinsic batch-lot and sample type variability. Accordingly, the ELISA-mode strategy, relevant controls, and a visual verification step are recommended. The single-antibody format proved unsatisfactory. It failed to detect the alpha subunit. Economically, it also requires relatively costly epoxy microplates and hydrolysis-prone F–NHS reagents. RedoxiFluor is much better-suited to the single-antibody format and allows percentage analysis. The holistic residue-weighted outcome metric cannot detect "balanced" changes. For instance, a 5% decrease in one cysteine and a 5% increase in another cancel out, which means important biology can be inadvertently missed. However, the holistic change can report changes occurring on as-yet m/s undetectable sites [102,103]. The orthogonality of ALISA to irreversibly oxidised chemotypes should be considered in oxidative distress settings when their formation might be appreciable. We recommend direct reactivity strategies to study them to better understand how oxidative distress chemically manifests. Carefully considering the cons and accounting for them with appropriate controls allows potential users to capitalise on the pros by properly implementing ALISA.

Future work can improve ALISA. To maximise sensitivity and time-efficiency, one may integrate ELISA-mode ALISA with the protein A format. Using smart-enzymes and protein A columns to purify the biotin-conjugated Fab_2-domain of the detector antibody would be an effective way of rendering it orthogonal to protein A. Alternatively, simple-step™ ELISA kits can be used. Next-generation N-terminal selective labelling reagents like 2-pyridinecarboxylaldehyde may also advance the single-antibody format [104]. Carefully titrating the F-MAL signal at a set protein input could enable percentage analysis. A promising specificity strategy is to integrate ALISA and m/s using new smart-chemicals. Isotopic m/s analysis might be enabled by separating the cysteine-reactive warhead from the F-MAL via a chemically cleavable linker, such as dialkoxydiphenylsilane [105]. Or couple ALISA to microfluidic immunoassays [106–108]. They enable a visual 2-factor authentication system to be implemented without sacrificing sample n-plex. The 2-factors comprise the molecular mass of the target, signal discrimination by separation, and the biotin-conjugated detector antibody. The proposed improvements can amplify the key strengths of ALISA, nullify weaknesses, and even lead to new analytical capabilities.

4. Conclusion

Performance benchmarking revealed the potential of ALISA for quantifying target-specific cysteine oxidation to advance understanding of redox-regulation and oxidative stress in diverse biological contexts. Confidence in the "unseen" microplate results was established by the "seeing-is-believing" orthogonal visual display approach.

5. Methods

5.1. Materials, reagents, and ethical approval

The details of the relevant materials and reagents used are provided throughout and altogether in the supplement (see Supplementary Table 1). We received full institutional ethical approval for the *X. laevis* (#ETH2021-0222) and human studies (#OL-ETHSHE-1436). The latter fully conformed to the Declaration of Helsinki.

5.2. Cell culture

Human-derived THP-1 cells (ECACC, UK, #88081201) were cultured (95% air, 5% CO_2, at 37 °C) in RPMI 1640 medium (ThermoFisher, UK, #11875093) supplemented with 10% fetal bovine serum, 2000 mg/L glucose, 2 mM L-glutamine and 1% penicillin/streptomycin, and maintained at densities between 2.5 and 9 × 10^5 cells/ml. To differentiate them into a macrophage-like phenotype, cells seeded at a density of 5 × 10^5 cells/ml were treated with 5 ng/ml PMA (Fisher Scientific, UK, #15476069). After 72 h, cells were gently rinsed with PBS and left to rest with fresh untreated media for 24 h.

5.3. Exercise study

After fasting overnight and warming-up at 50 W (W) for 5 min, eight healthy human male ($n = 8$, age = 38 ± 9 years, height = 179.3 ± 5.8 cm, mass = 79.9 ± 9.5 kg, maximal oxygen uptake = 47.4 ± 5.7 ml/kg/min^{-1}, max work rate = 946 ± 78 W) participants completed an incremental exercise test to exhaustion on a bicycle ergometer (Lode Corival, Groningen, The Netherlands). The incremental test commenced at an initial work rate of 50 W and increased by 20 W min^{-1} in a ramp based linear protocol until volitional exhaustion [65]. All tests were performed at a similar time of day in a temperature regulated environment (~22 °C). Venous blood samples were collected pre and post exercise via venepuncture into an EDTA-vacutainer containing 100 mM NEM. NEM-alkylated erythrocytes were lysed in ice-cold buffer (25 mM Tris-HCl, 150 mM NaCl, 1 mM EDTA, 1% NP-40, 5% glycerol, pH 7.1, ThermoFisher, UK, #87787) supplemented with a protease inhibitor tablet (Sigma Aldrich, UK, #11697498001) and centrifuged at 12,000 *g* for 5 min at RT to remove insoluble material. The soluble supernatants were used for cysteine labelling.

5.4. Xenopus laevis

In line with previous work [74], unfertilised eggs were harvested from two different adult *X. laevis* females housed at 18 °C in groups of 20 (i.e., each *X. laevis* sample represents the weighted mean of 20 eggs). Although it is possible to perform biochemical analysis in 1-cell samples, groups of 20 were used to amplify technical differences by minimising biological variability. Adult females were maintained on a trout diet under standard husbandry conditions at the European *Xenopus* Resource Centre (EXRC, https://xenopusresource.org/). Samples were lysed in ice-cold buffer (as above) supplemented with a protease inhibitor tablet and the appropriate alkylating agent. They were then centrifuged at 5000 *g* for 5 min at RT to remove insoluble material. The *g* value was decreased to limit the amount of soluble yolk protein.

5.5. Cysteine labelling

Reversibly oxidised cysteines were labelled for ALISA by (1) alkylating reduced cysteines with NEM (ThermoFisher, UK, #23030, 100 mM erythrocytes, 10 mM THP-1 cells and *X. laevis*) immediately at lysis, (2) reducing reversibly oxidised cysteines with 5 mM neutral-TCEP (Sigma, UK, #580561), and (3) labelling the newly reduced cysteines with 1 mM F-MAL1 (fluorescin-5-maleimide, ThermoFisher, UK, #62245). The cysteine labelling procedure for RedoxiFluor involved (1) alkylating reduced cysteines with 0.75 mM F-MAL1, (2) reducing reversibly oxidised cysteines with 5 mM neutral-TCEP before (3) decorating them with 0.5 mM F-MAL2 (AlexaFluor™647-C_2-maleimide, ThermoFisher, UK, #A20347). The cysteine labelling procedure was the same for Click-PEG except the F-MAL2 label was replaced with *trans*-cyclooctene PEG3 maleimide (TPN, Sigma, UK, #790445). Regardless of the method, the incubation steps were performed in the dark for 30 min

at 4 °C with the samples being vortexed for 5–10 s at 5 min intervals to ensure mixing. Before new cysteine-reactive compounds were added, excess alkylating or reducing agents were removed by size exclusion chromatography with a 6 kDa cut-off spin column (Bio-Rad, UK, #7326222).

5.6. Cysteine redox state standards

Fully labelled F-MAL1/2 standards were prepared by simplifying the cysteine labelling procedure to a single colour (e.g., TCEP→F-MAL1) [80]. 100%-Standards were mixed as appropriate to produce the 10–90% reversibly oxidised redox states (e.g., for a 10 μl final volume, 9 μl of 100%-F-MAL1 was mixed with 1 μl of 100%-F-MAL2 to prepare the 90% oxidised standard).

5.7. Internal pass/fail performance benchmarking

To internally performance benchmark each assay, the cysteine redox state standards were used in the following experiments.

a. **Binding.** The ability to detect the analyte was determined by running the assay and evidenced using the F-MAL and/or HRP signal outputs per the assay format. To evaluate the impact of the alkylating agent used on epitope-paratope recognition, 100% F-MAL1, NEM, or F-MAL2 labelled standards were analysed alongside unlabelled samples as appropriate.
b. **Sensitivity.** Sensitivity was determined alongside binding in a dose-response format by adding 0.5, 1, 2, 4 or 8 μg of 100% labelled sample.
c. **Accuracy.** Accuracy was analysed by using the cysteine redox state standards to determine whether the assay could quantify target-specific percent oxidation within 5% of the standard. For example, for the 40% oxidised standard, an experimental value of 42 and 46% would pass and fail, respectively.
d. **Reliability.** Reliability was assessed in sample standards by quantifying the inter-assay and intra-assay CV values.
e. **Specificity.** Three different tests were used to appraise the specificity of the assay. First, in ELISA-mode experiments the positive HRP signal was used to confirm target-specific binding. Second, immunodepleted samples were used to test the specificity of the assay via the HRP and F-MAL readouts. For PRDX2 and the alpha subunit, Hela lysates (Abcam, UK, #ab170197) and human erythrocytes were used for technical reasons. For example, the alpha subunit is so abundant in *X. laevis* it is difficult to fully deplete without excessive reagent consumption hence samples lacking mitochondria were used. Third, specificity was tested by analysing the F-MAL and/or HRP signals in sham rabbit immunoglobin treated wells. For all experiments, 100% F-MAL1 standards were used.

5.8. ALISA antibodies and biotin-conjugation procedures

For the ELISA-mode ALISA assays, a PRDX2 kit (R&D systems, UK, #DY3489-05) and bovine serum albumin (BSA) and azide free matched-pair antibody kits (Abcam, UK) for CDK6 (#ab253747), Aurora B (#ab253800), and CDC25C (#ab244070) were used. For GAPDH, separate capture (Abcam, UK, #ab252636) and detector (Abcam, UK, #ab276013) antibodies were purchased. The label-free detector antibodies were biotin-conjugated using a lightning-link® kit (Abcam, UK, #ab201795) according to the manufacturer's method.

5.9. ELISA-mode ALISA

To perform ELISA-mode ALISA [8], black Nunc®MaxiSorp™ 96-well microplates (ThermoFisher, UK, #15155) were incubated with 2 μg/ml capture antibody overnight at 4 °C in binding buffer (35 mM $NaHCO_3$, 15 mM Na_2CO_3, pH 9.6), blocked with Superblock™, and washed (3 × 2 min PBST washes at 400 rpm). Recombinant standards (recombinant GAPDH, ThermoFisher, UK #LF-P0008) and samples (diluted in 0.5% PBST supplemented with 10% Superblock™) were added in duplicate and incubated for 2 h at RT. After removing unbound standard/sample, wells were washed (3 × 2 min PBST washes), probed with 0.5 μg/ml biotin-conjugated detector antibody for 1 h at RT, and washed. Then 0.05 μg/ml of HRP-conjugated streptavidin was added for 1 h at RT. After a wash step, wells were incubated with QuantaBlu™ working reagent (ThermoFisher, UK, #P9416), prepared according to the manufacturer's instructions, until the signal developed. The QuantaBlu™ signal was measured at 325 and 425 nm for 100 ms. Denaturing buffer (4% SDS in ddH_2O) was used to unmask the F-MAL1 signal (i.e., to prevent the antibody-target complex from optically obscuring the quantum excitation of the fluorescent groups). After subtracting the background, target-specific cysteine redox state was calculated as: F-MAL/[target]. All steps were performed in the dark and fluorescent signals were read in a dark room.

5.10. Single antibody mode ALISA

To perform the single antibody mode ALISA assay [8], epoxy group derivatised microplates (PolyAn, Germany, #00695251) were treated with 100 ng of alpha subunit capture antibody in binding buffer (Na_2HPO_4, 50 mM NaCl, pH 8.5) overnight at 4 °C with gentle agitation. The epoxy groups covalently bond the capture antibody via strain-promoted nucleophilic substitution chemistry. Unreacted epoxy groups were blocked in binding buffer supplemented with 5 mM glycine for 90 min at RT. After washing the wells (4 × 2 min PBST washes), samples were added for 2 h at RT with gentle agitation in the dark. Unbound sample was removed by washing (3 × 2 min PBST washes) before the bound target-antibody immunocomplexes were treated with 350 μM AlexaFluor™647-NHS (ThermoFisher, UK, #A37573) in PBS for 30 min at RT. Following a wash step (3 × 2 min with PBST), the target was separated from the covalently bound capture antibody via elution buffer. Eluents were transferred to a black microplate and the fluorescent signals were measured on a microplate reader at the appropriate wavelengths for 100 ms.

For the protein A mode ALISA experiments, the capture antibody was passively bound to the plate as per the RedoxiFluor section below. Either F–NHS was applied after the sample binding step or the samples were pre-treated with F–NHS. For the latter protocol, excess F–NHS was removed with a spin column and samples lysed in amine-free HEPES buffer were used.

5.11. Global mode ALISA

To run ALISA in global mode to quantify the redox state of the wider proteome in THP-1 cells, 1 μl of F-MAL labelled lysate was added in triplicate to 99 μl ddH_2O in a black microplate. Cysteine redox state was calculated by dividing the F-MAL value by the total protein value of the sample, as determined by a BCA assay (e.g., F-MAL/total protein). Global mode ALISA was performed in erythrocytes by dividing the F-MAL value relative to haemoglobin absorbance at 577 nm [65].

5.12. Protein a mode RedoxiFluor

To determine the cysteine redox state of the alpha subunit using protein A mode RedoxiFluor [80], 100 ng of capture antibody (Abcam, UK, #ab14748) in binding buffer (50%: 0.05% Tween20® TBST; 50% SuperBlock™) was added to the wells of a black protein A functionalised microplate (ThermoFisher, UK, #15155) for 1 h at RT with gentle agitation. Note protein A can bind mouse IgG2b subtypes like the selected capture antibody. Unbound capture antibody was removed by washing in 0.05% TBST (3 × 2 min washes). Assay standards and samples (diluted in 0.5% PBST 10% Superblock™) were added for 2 h at RT. After removing unbound samples, the washed wells were incubated

with denaturing buffer. The F-MAL1 and F-MAL2 signals were measured on a microplate reader for 100 ms with a bandwidth of 5 nm. After subtracting the background, target-specific cysteine redox state values were calculated in percentages (e.g., reduced = F-MAL1/[F-MAL1 + F-MAL2]*100) after correcting (c) the F-MAL1 and F-MAL2 signals for their different quantum yields (q) and extinction co-efficient (e) values using the equation:

$$c - F - MAL = [(F - MAL * q) / e].$$

5.13. Chemotype-specific study

For the chemotype-specific study reported in Fig. 6, *X. laevis* eggs were lysed and reduced with 5 mM TCEP. After removing excess TCEP, aliquots (50 μg) were incubated with 1 μg recombinant xanthine oxidase (Sigma, UK, #X4500) and 0.1 mM hypoxanthine (Sigma, UK, #H9377) for 30 min with or without 5 mM GSSG (Sigma, UK, #G2299) [89]. In some experiments, 500 ng of bovine CuZnSOD (Sigma, UK, #574594) and CAT (Sigma, UK, #C9322) were added to prevent reversible cysteine oxidation by metabolising xanthine oxidase-derived superoxide and hydrogen peroxide. To selectively detect RSSG, the samples were treated with NEM to block reduced thiols. After removing excess NEM, 2.5 μg E. *coli* mutant GRX3 (IMCO corporation, Sweden, #GRX-05), 1 mM glutathione (Sigma, UK, #G6529), 1 mM NADPH (Sigma, UK, #10107824001), and 4 U/ml glutathione reductase from Bakers' yeast (Sigma, UK, #G3664) were added for 30 min [90]. After a spin column step, 1 mM F-MAL was added for 30 min. To account for the inability to remove the ectopic enzymes using a spin column, their degree of F-MAL labelling was calculated separately and subtracted from the experimental sample. Global and ELISA mode ALISA were performed. For the PPP2CA-specific analysis, a matched-pair ELISA kit was used (Abcam, UK, #218147).

5.14. The dimer assay

The dimer assays were performed in NEM-alkylated THP-1 lysates under non-reducing SDS-PAGE conditions. PRDX2 and PRDX1 cysteine redox states (%RSSR) were quantified in an internally normalised way by calculating the percentage of monomeric and dimeric protein relative to the total signal (total = monomer + dimer).

5.15. Modified cysteinyl labelling assay

To perform the modified cysteinyl labelling assay, GAPDH capture antibody aliquots (5 μg) were incubated with 30 μl of protein A-conjugated magnetic Dynabeads™ in PBST (0.25% Tween-20®) for 1 h at 24 °C with gentle agitation. Unbound antibody was removed, beads were washed (3 x PBST) and incubated with the F-MAL labelled samples for 2 h at 21 °C. Washed beads were incubated in non-reducing bromophenol blue-free 4X loading buffer for 1 h at 37 °C with gentle agitation. An immunoblot procedure was followed (see below) with the exception that the F-MAL signal was visualised and quantified after the blocking step (i.e., to prevent the streptavidin-conjugate optically masking it). Membranes were probed with the biotin-conjugated GAPDH detector antibody (1:1000) overnight at RT, washed, probed with AlexaFluor™647-conjugated streptavidin (1:2000, ThermoFisher, UK, #S21374) for 1 h at RT, washed, and visualised. GAPDH-specific cysteine redox state was quantified as: F-MAL (i.e., cysteine)/streptavidin-AlexaFluor™647 (i.e., GAPDH).

5.16. Click-PEG

To perform the Click-PEG assay [27], 50 μg of NEM-alkylated lysates were labelled with 2.5 mM TPN in the presence of 5 mM neutral-TCEP. Excess TPN and TCEP were removed, before the IEDDA reaction was initiated by adding 1 mM 6-methyltetrazine PEG-5000 (Tz-PEG5, Click chemistry tools, USA, #1090) for 60 min at RT. Click-reacted samples were analysed by immunoblot expect with the mouse alpha subunit antibody was detected using a fluorescent-conjugated secondary antibody (AlexaFluor™750, Abcam, UK, #ab175741). For the band analysis, the amount of reduced (i.e., unshifted) to reversibly oxidised protein (i.e., mass shifted) protein was quantified in percentages. To correct for the middle alpha subunit band representing a 50% cysteine redox state (i.e., 1 reduced and 1 oxidised cysteine), the signal was divided into 2 and added to the reduced and oxidised columns. The ratio-metric band analysis procedures were per previous research [24–27].

5.17. Immunoblot

To immunoblot a target, proteins were resolved to their pore size limit on precast 4–15% gradient polyacrylamide gels in SDS-PAGE (Bio-Rad, UK, #4561085). Gels were transferred to 0.45 μM low autofluorescence PVDF membranes (Bio-Rad, UK, #1620261). Membranes were blocked in non-fat dry milk (NFDM) for at least 1 h at RT, probed with target-specific antibodies (diluted in TBST containing 5% Superblock™) overnight at RT, washed (3 × 5 min TBST), and probed with a species-specific alkaline phosphatase-conjugated secondary antibody (Abcam, UK, #ab97048) for 1 h at RT, washed (3 × 5 min), incubated with BCIP®/NBT substrate (Sigma, UK, #B5655) until visible bands appeared, and visualised on an Analytik Jena scanner. The primary PRDX2 (Abcam, UK, #ab109367), PRDX1 (Abcam, UK, #ab41906), and PRDX-SO_3 (Abcam, UK, #ab16830) antibodies were used at 1:100 dilution. The bands were quantified on proprietary VisionWorks™ software.

6. IP

To enrich or immunodeplete a target [80], capture antibody aliquots were incubated with PBST-washed protein A magnetic Dynabeads™ (ThermoFisher, UK, #10002D), according to the species of origin, functionalised magnetic beads for 1 h at RT in 0.5% PBST. After removing unbound antibody by washing, the capture antibody-bead complexes were incubated with undiluted samples (75–150 μg) for 4 h at RT. The amount of sample added for immuno-depletion experiments was small (1 μg) to allow for near complete capture. The immune-depleted sample was used for ALISA or RedoxiFluor. In the IP experiments, the captured sample was used for the modified cysteinyl labelling assay.

6.1. Flow cytometry

THP-1 monocytes and macrophages were collected, washed with PBS, and resuspended in 1 M PBS, 0.1% sodium azide, pH 7.4. Samples containing 1×10^6 cells were first labelled with 0.5% Zombie Violet™ (Biolegend, USA, #423113) at RT for 30 min. Then washed with protein-free labelling buffer to remove the excess dye, resuspended with ice-cold labelling buffer (PBS, 0.1% sodium azide, 1% BSA, pH 7.4) supplemented with anti-CD14-FITC (BD Biosciences, USA, #555397) and/or anti-CD36-APC antibodies (Biolegend, USA, #336207), or their corresponding isotype controls (BD Biosciences, USA #555573, Biolegend, USA #400221), and incubated on ice for 30 min. Unbound antibodies were removed by washing, cells were resuspended with ice-cold labelling buffer, and analysed using MACSQuant® Analyzer 10 Flow Cytometer (Miltenyi Biotec, UK). Flow cytometry data were analysed using FlowJo software (BD Biosciences, USA). Cells were gated by plotting side scatter area (SSC-A) vs forward scatter area (FSC-A). Single cells were selected by plotting side scatter hight (SSC–H) vs SSC-A. Membrane compromised cells were discriminated from viable ones by plotting SSC-A vs Zombie Violet™, where heat-killed cells (65 °C for 5 min) were used as a positive control. For the surface marker experiments, single-stained controls and isotype controls were utilised to establish

gates and calculate percentage positivity. Geometric mean fluorescence intensity (MFI) for each marker was normalised by subtracting the appropriate control (see Supplementary Fig. 2).

6.2. Microscopy

THP-1 monocytes and macrophages were qualitatively assessed for proliferation and adherence by phase-contrast microscopy using a Lecia Dmi8 microscope (Lecia, Germany, Europe). Cells were imaged with 20× objective at 0, 72 and 96 h post-PMA treatment. An automated stage control function imaged the same location on the plate each time.

6.3. Statistical analysis

Data-set normality was assessed using Shapiro-Wilk and Kolmogorov-Smirnov testing and the experimental design appropriate parametric or non-parametric tests were performed with alpha $P \leq 0.05$ using GraphPad Prism Version 9 (https://www.graphpad.com). When a 1-way ANOVA or non-parametric test was used and post-hoc pair-wise comparison tests, such as the Tukey test, were applied as appropriate. The figure legends report the exact statistical test used. Data are presented as Mean (M) and Standard Deviation (SD).

Author contributions: CREDIT statement

Ahmet Tuncay: Investigation, Data curation, Formal analysis, Writing- Reviewing and Editing; **Daniel R. Crabtree**: Investigation, Formal analysis, Data curation, Visualisation, Writing- Reviewing and Editing; **David J. Muggeridge**: Investigation, Resources, Writing- Reviewing and Editing; **Holger Husi**: Supervision, Writing- Reviewing and Editing; **James N. Cobley**: Conceptualisation; Methodology, Supervision, Investigation, Visualisation, Writing- Original draft preparation; Writing- Reviewing and Editing.

Declaration of competing interest

There are no conflicts of interest.

Acknowledgements

We thank Professor Matthew Guille, Dr Anna Noble, and their colleagues at the European *Xenopus* Resource Centre (EXRC) for kindly providing the *X. laevis* samples. The graphical abstract, Figs. 1, 2A and 4A were created using Biorender (http://www.Biorender.com) and exported with a publication license.

Appendix A. Supplementary data

Supplementary data to this article can be found online at https://doi.org/10.1016/j.freeradbiomed.2023.05.006.

References

[1] J.M. Held, Redox systems biology: harnessing the sentinels of the cysteine redoxome, Antioxidants Redox Signal. 32 (2020) 659–676, https://doi.org/10.1089/ars.2019.7725.
[2] B. D'Autréaux, M.B. Toledano, ROS as signalling molecules: mechanisms that generate specificity in ROS homeostasis, Nat. Rev. Mol. Cell Biol. 8 (2007) 813–824, https://doi.org/10.1038/nrm2256.
[3] K.M. Holmström, T. Finkel, Cellular mechanisms and physiological consequences of redox-dependent signalling, Nat. Rev. Mol. Cell Biol. 15 (2014) 411–421, https://doi.org/10.1038/nrm3801.
[4] H. Sies, D.P. Jones, Reactive oxygen species (ROS) as pleiotropic physiological signalling agents, Nat. Rev. Mol. Cell Biol. 21 (2020) 363–383, https://doi.org/10.1038/s41580-020-0230-3.
[5] A. Salmeen, J.N. Andersen, M.P. Myers, T.-C. Meng, J.A. Hinks, N.K. Tonks, D. Barford, Redox regulation of protein tyrosine phosphatase 1B involves a sulphenyl-amide intermediate, Nature 423 (2003) 769–773, https://doi.org/10.1038/nature01680.
[6] C.E. Paulsen, K.S. Carroll, Cysteine-Mediated redox signaling: chemistry, biology, and tools for discovery, Chem. Rev. 113 (2013) 4633–4679, https://doi.org/10.1021/cr300163e.
[7] H. Xiao, M.P. Jedrychowski, D.K. Schweppe, E.L. Huttlin, Q. Yu, D.E. Heppner, J. Li, J. Long, E.L. Mills, J. Szpyt, Z. He, G. Du, R. Garrity, A. Reddy, L.P. Vaites, J. A. Paulo, T. Zhang, N.S. Gray, S.P. Gygi, E.T. Chouchani, A quantitative tissue-specific landscape of protein redox regulation during aging, Cell 180 (2020) 968–983, https://doi.org/10.1016/j.cell.2020.02.012, e24.
[8] A. Noble, M. Guille, J.N. Cobley, ALISA: a microplate assay to measure protein thiol redox state, Free Radical Biol. Med. 174 (2021) 272–280, https://doi.org/10.1016/j.freeradbiomed.2021.08.018.
[9] E. Marcon, H. Jain, A. Bhattacharya, H. Guo, S. Phanse, S. Pu, G. Byram, B. C. Collins, E. Dowdell, M. Fenner, X. Guo, A. Hutchinson, J.J. Kennedy, B. Krastins, B. Larsen, Z.-Y. Lin, M.F. Lopez, P. Loppnau, S. Miersch, T. Nguyen, J. B. Olsen, M. Paduch, M. Ravichandran, A. Seitova, G. Vadali, M.S. Vogelsang, J. R. Whiteaker, G. Zhong, N. Zhong, L. Zhao, R. Aebersold, C.H. Arrowsmith, A. Emili, L. Frappier, A.-C. Gingras, M. Gstaiger, A.G. Paulovich, S. Koide, A. A. Kossiakoff, S.S. Sidhu, S.J. Wodak, S. Gräslund, J.F. Greenblatt, A.M. Edwards, Assessment of a method to characterize antibody selectivity and specificity for use in immunoprecipitation, Nat. Methods 12 (2015) 725–731, https://doi.org/10.1038/nmeth.3472.
[10] V. Marx, Finding the right antibody for the job, Nat. Methods 10 (2013) 703–707, https://doi.org/10.1038/nmeth.2570.
[11] M. Uhlen, A. Bandrowski, S. Carr, A. Edwards, J. Ellenberg, E. Lundberg, D. L. Rimm, H. Rodriguez, T. Hiltke, M. Snyder, T. Yamamoto, A proposal for validation of antibodies, Nat. Methods 13 (2016) 823–827, https://doi.org/10.1038/nmeth.3995.
[12] H. Sies, V.V. Belousov, N.S. Chandel, M.J. Davies, D.P. Jones, G.E. Mann, M. P. Murphy, M. Yamamoto, C. Winterbourn, Defining roles of specific reactive oxygen species (ROS) in cell biology and physiology, Nat. Rev. Mol. Cell Biol. (2022) 1–17, https://doi.org/10.1038/s41580-022-00456-z.
[13] H. Kim, S. Ha, H.Y. Lee, K. Lee, ROSics: chemistry and proteomics of cysteine modifications in redox biology, Mass Spectrom. Rev. 34 (2015) 184–208, https://doi.org/10.1002/mas.21430.
[14] J.N. Cobley, H. Husi, Immunological techniques to assess protein thiol redox state: opportunities, challenges and solutions, Antioxidants 9 (2020) 315, https://doi.org/10.3390/antiox9040315.
[15] H. Sies, C. Berndt, D.P. Jones, Oxidative stress, Annu. Rev. Biochem. 86 (2016) 1–34, https://doi.org/10.1146/annurev-biochem-061516-045037.
[16] H. Sies, Oxidative Stress, Academic Press, 2019.
[17] H. Sies, Oxidative eustress: on constant alert for redox homeostasis, Redox Biol. 41 (2021), 101867, https://doi.org/10.1016/j.redox.2021.101867.
[18] J.N. Cobley, M.L. Fiorello, D.M. Bailey, 13 reasons why the brain is susceptible to oxidative stress, Redox Biol. 15 (2018) 490–503, https://doi.org/10.1016/j.redox.2018.01.008.
[19] J.N. Cobley, Synapse pruning: mitochondrial ROS with their hands on the shears, Bioessays 40 (2018), 1800031, https://doi.org/10.1002/bies.201800031.
[20] H.J. Forman, H. Zhang, Targeting oxidative stress in disease: promise and limitations of antioxidant therapy, Nat. Rev. Drug Discov. (2021) 1–21, https://doi.org/10.1038/s41573-021-00233-1.
[21] M.P. Murphy, H. Bayir, V. Belousov, C.J. Chang, K.J.A. Davies, M.J. Davies, T. P. Dick, T. Finkel, H.J. Forman, Y. Janssen-Heininger, D. Gems, V.E. Kagan, B. Kalyanaraman, N.-G. Larsson, G.L. Milne, T. Nyström, H.E. Poulsen, R. Radi, H. V. Remmen, P.T. Schumacker, P.J. Thornalley, S. Toyokuni, C.C. Winterbourn, H. Yin, B. Halliwell, Guidelines for measuring reactive oxygen species and oxidative damage in cells and in vivo, Nat Metabolism 4 (2022) 651–662, https://doi.org/10.1038/s42255-022-00591-z.
[22] B. Boivin, S. Zhang, J.L. Arbiser, Z.-Y. Zhang, N.K. Tonks, A modified cysteinyl-labeling assay reveals reversible oxidation of protein tyrosine phosphatases in angiomyolipoma cells, Proc. Natl. Acad. Sci. USA 105 (2008) 9959–9964, https://doi.org/10.1073/pnas.0804336105.
[23] A.D. Londhe, A. Bergeron, S.M. Curley, F. Zhang, K.D. Rivera, A. Kannan, G. Coulis, S.H.M. Rizvi, S.J. Kim, D.J. Pappin, N.K. Tonks, R.J. Linhardt, B. Boivin, Regulation of PTP1B activation through disruption of redox-complex formation, Nat. Chem. Biol. 16 (2020) 122–125, https://doi.org/10.1038/s41589-019-0433-0.
[24] L. Makmura, M. Hamann, A. Areopagita, S. Furuta, A. Muoz, J. Momand, Development of a sensitive assay to detect reversibly oxidized protein cysteine sulfhydryl groups, Antioxidants Redox Signal. 3 (2001) 1105–1118, https://doi.org/10.1089/152308601317203611.
[25] J.R. Burgoyne, O. Oviosu, P. Eaton, The PEG-switch assay: a fast semi-quantitative method to determine protein reversible cysteine oxidation, J. Pharmacol. Toxicol. 68 (2013) 297–301, https://doi.org/10.1016/j.vascn.2013.07.001.
[26] L.A.G. van Leeuwen, E.C. Hinchy, M.P. Murphy, E.L. Robb, H.M. Cochemé, Click-PEGylation – a mobility shift approach to assess the redox state of cysteines in candidate proteins, Free Radical Biol. Med. 108 (2017) 374–382, https://doi.org/10.1016/j.freeradbiomed.2017.03.037.
[27] J.N. Cobley, A. Noble, E. Jimenez-Fernandez, M.-T.V. Moya, M. Guille, H. Husi, Catalyst-free Click PEGylation reveals substantial mitochondrial ATP synthase sub-unit alpha oxidation before and after fertilisation, Redox Biol. 26 (2019), 101258, https://doi.org/10.1016/j.redox.2019.101258.
[28] C.C. Winterbourn, Reconciling the chemistry and biology of reactive oxygen species, Nat. Chem. Biol. 4 (2008) 278–286, https://doi.org/10.1038/nchembio.85.

[29] B.C. Dickinson, C.J. Chang, Chemistry and biology of reactive oxygen species in signaling or stress responses, Nat. Chem. Biol. 7 (2011) 504–511, https://doi.org/10.1038/nchembio.607.

[30] S. Parvez, M.J.C. Long, J.R. Poganik, Y. Aye, Redox signaling by reactive electrophiles and oxidants, Chem. Rev. 118 (2018) 8798–8888, https://doi.org/10.1021/acs.chemrev.7b00698.

[31] P.A. Karplus, A primer on peroxiredoxin biochemistry, Free Radical Biol. Med. 80 (2015) 183–190, https://doi.org/10.1016/j.freeradbiomed.2014.10.009.

[32] Z.A. Wood, L.B. Poole, P.A. Karplus, Peroxiredoxin evolution and the regulation of hydrogen peroxide signaling, Science 300 (2003) 650–653, https://doi.org/10.1126/science.1080405.

[33] J. Bolduc, K. Koruza, T. Luo, J.M. Pueyo, T.N. Vo, D. Ezeriņa, J. Messens, Peroxiredoxins wear many hats: factors that fashion their peroxide sensing personalities, Redox Biol. 42 (2021), 101959, https://doi.org/10.1016/j.redox.2021.101959.

[34] C.C. Winterbourn, Biological production, detection, and fate of hydrogen peroxide, Antioxidants Redox Signal. 29 (2018) 541–551, https://doi.org/10.1089/ars.2017.7425.

[35] J.J. Skoko, J. Cao, D. Gaboriau, M. Attar, A. Asan, L. Hong, C.E. Paulsen, H. Ma, Y. Liu, H. Wu, C.M. Furdui, Y. Manevich, C.G. Morrison, E.T. Brown, D. Normolle, M. Spies, M.A. Spies, K. Carroll, C.A. Neumann, Redox regulation of RAD51 Cys319 and homologous recombination by peroxiredoxin 1, Redox Biol. (2022), 102443, https://doi.org/10.1016/j.redox.2022.102443.

[36] M. Herb, M. Schramm, Functions of ROS in macrophages and antimicrobial immunity, Antioxidants 10 (2021) 313, https://doi.org/10.3390/antiox10020313.

[37] E.L. Mills, D.G. Ryan, H.A. Prag, D. Dikovskaya, D. Menon, Z. Zaslona, M. P. Jedrychowski, A.S.H. Costa, M. Higgins, E. Hams, J. Szpyt, M.C. Runtsch, M. S. King, J.F. McGouran, R. Fischer, B.M. Kessler, A.F. McGettrick, M.M. Hughes, R.G. Carroll, L.M. Booty, E.V. Knatko, P.J. Meakin, M.L.J. Ashford, L.K. Modis, G. Brunori, D.C. Sévin, P.G. Fallon, S.T. Caldwell, E.R.S. Kunji, E.T. Chouchani, C. Frezza, A.T. Dinkova-Kostova, R.C. Hartley, M.P. Murphy, L.A. O'Neill, Itaconate is an anti-inflammatory metabolite that activates Nrf2 via alkylation of KEAP1, Nature 556 (2018) 113–117, https://doi.org/10.1038/nature25986.

[38] M.A. Forrester, H.J. Wassall, L.S. Hall, H. Cao, H.M. Wilson, R.N. Barker, M. A. Vickers, Similarities and differences in surface receptor expression by THP-1 monocytes and differentiated macrophages polarized using seven different conditioning regimens, Cell. Immunol. 332 (2018) 58–76, https://doi.org/10.1016/j.cellimm.2018.07.008.

[39] S.R. Jaffrey, S.H. Snyder, The biotin switch method for the detection of S-nitrosylated proteins, Sci. STKE (2001) pl1, https://doi.org/10.1126/stke.2001.86.pl1, 2001.

[40] R.E. Hansen, J.R. Winther, An introduction to methods for analyzing thiols and disulfides: reactions, reagents, and practical considerations, Anal. Biochem. 394 (2009) 147–158, https://doi.org/10.1016/j.ab.2009.07.051.

[41] J.R. Winther, C. Thorpe, Quantification of thiols and disulfides, Biochimica Et Biophysica Acta Bba - Gen Subj. 1840 (2014) 838–846, https://doi.org/10.1016/j.bbagen.2013.03.031.

[42] L.B. Poole, C.M. Furdui, S.B. King, Introduction to approaches and tools for the evaluation of protein cysteine oxidation, Essays Biochem. 64 (2020) 1–17, https://doi.org/10.1042/ebc20190050.

[43] B. Biteau, J. Labarre, M.B. Toledano, ATP-dependent reduction of cysteine–sulphinic acid by S. cerevisiae sulphiredoxin, Nature 425 (2003) 980–984, https://doi.org/10.1038/nature02075.

[44] A.V. Peskin, P.E. Pace, J.B. Behring, L.N. Paton, M. Soethoudt, M.M. Bachschmid, C.C. Winterbourn, Glutathionylation of the active site cysteines of peroxiredoxin 2 and recycling by glutaredoxin, J. Biol. Chem. 291 (2016) 3053–3062, https://doi.org/10.1074/jbc.m115.692798.

[45] A.A. Bradlaugh, G. Fedele, A.L. Munro, C.N. Hansen, J.M. Hares, S. Patel, C. P. Kyriacou, A.R. Jones, E. Rosato, R.A. Baines, Essential elements of radical pair magnetosensitivity in Drosophila, Nature 615 (2023) 111–116, https://doi.org/10.1038/s41586-023-05735-z.

[46] M.P. Murphy, A. Holmgren, N.-G. Larsson, B. Halliwell, C.J. Chang, B. Kalyanaraman, S.G. Rhee, P.J. Thornalley, L. Partridge, D. Gems, T. Nyström, V. Belousov, P.T. Schumacker, C.C. Winterbourn, Unraveling the biological roles of reactive oxygen species, Cell Metabol. 13 (2011) 361–366, https://doi.org/10.1016/j.cmet.2011.03.010.

[47] B. Halliwell, M. Whiteman, Measuring reactive species and oxidative damage in vivo and in cell culture: how should you do it and what do the results mean? Br. J. Pharmacol. 142 (2004) 231–255, https://doi.org/10.1038/sj.bjp.0705776.

[48] B. H, J. Gutteridge, Free Radicals in Biology and Medicine, 2015.

[49] H.J. Forman, O. Augusto, R. Brigelius-Flohe, P.A. Dennery, B. Kalyanaraman, H. Ischiropoulos, G.E. Mann, R. Radi, L.J. Roberts, J. Vina, K.J.A. Davies, Even free radicals should follow some rules: a Guide to free radical research terminology and methodology, Free Radical Biol. Med. 78 (2015) 233–235, https://doi.org/10.1016/j.freeradbiomed.2014.10.504.

[50] N.V. Margaritelis, J.N. Cobley, V. Paschalis, A.S. Veskoukis, A.A. Theodorou, A. Kyparos, M.G. Nikolaidis, Going retro: oxidative stress biomarkers in modern redox biology, Free Radical Biol. Med. 98 (2016) 2–12, https://doi.org/10.1016/j.freeradbiomed.2016.02.005.

[51] J.N. Cobley, G.L. Close, D.M. Bailey, G.W. Davison, Exercise redox biochemistry: conceptual, methodological and technical recommendations, Redox Biol. 12 (2017) 540–548, https://doi.org/10.1016/j.redox.2017.03.022.

[52] JamesN. Cobley, G.W. Davison, Oxidative Eustress in Exercise Physiology, CRC Press, 2022, https://doi.org/10.1201/9781003051619.

[53] C. Henríquez-Olguin, J.R. Knudsen, S.H. Raun, Z. Li, E. Dalbram, J.T. Treebak, L. Sylow, R. Holmdahl, E.A. Richter, E. Jaimovich, T.E. Jensen, Cytosolic ROS production by NADPH oxidase 2 regulates muscle glucose uptake during exercise, Nat. Commun. 10 (2019) 4623, https://doi.org/10.1038/s41467-019-12523-9.

[54] C. Henriquez-Olguin, R. Meneses-Valdes, T.E. Jensen, Compartmentalized muscle redox signals controlling exercise metabolism – current state, future challenges, Redox Biol. 35 (2020), 101473, https://doi.org/10.1016/j.redox.2020.101473.

[55] J.N. Pugh, C. Stretton, B. McDonagh, P. Brownridge, A. McArdle, M.J. Jackson, G. L. Close, Exercise stress leads to an acute loss of mitochondrial proteins and disruption of redox control in skeletal muscle of older subjects: an underlying decrease in resilience with aging? Free Radical Biol. Med. 177 (2021) 88–99, https://doi.org/10.1016/j.freeradbiomed.2021.10.003.

[56] S.K. Powers, M.J. Jackson, Exercise-induced oxidative stress: cellular mechanisms and impact on muscle force production, Physiol. Rev. 88 (2008) 1243–1276, https://doi.org/10.1152/physrev.00031.2007.

[57] J.N. Cobley, P.R. Moult, J.G. Burniston, J.P. Morton, G.L. Close, Exercise improves mitochondrial and redox-regulated stress responses in the elderly: better late than never, Biogerontology 16 (2015) 249–264, https://doi.org/10.1007/s10522-014-9546-8.

[58] J.N. Cobley, H. McHardy, J.P. Morton, M.G. Nikolaidis, G.L. Close, Influence of vitamin C and vitamin E on redox signaling: implications for exercise adaptations, Free Radical Biol. Med. 84 (2015) 65–76, https://doi.org/10.1016/j.freeradbiomed.2015.03.018.

[59] J.N. Cobley, G.K. Sakellariou, D.J. Owens, S. Murray, S. Waldron, W. Gregson, W. D. Fraser, J.G. Burniston, L.A. Iwanejko, A. McArdle, J.P. Morton, M.J. Jackson, G.L. Close, Lifelong training preserves some redox-regulated adaptive responses after an acute exercise stimulus in aged human skeletal muscle, Free Radical Biol. Med. 70 (2014) 23–32, https://doi.org/10.1016/j.freeradbiomed.2014.02.004.

[60] J.N. Cobley, Oxidative Stress (2020) 447–462, https://doi.org/10.1016/b978-0-12-818606-0.00023-7.

[61] N.V. Margaritelis, J.N. Cobley, V. Paschalis, A.S. Veskoukis, A.A. Theodorou, A. Kyparos, M.G. Nikolaidis, Principles for integrating reactive species into in vivo biological processes: examples from exercise physiology, Cell. Signal. 28 (2016) 256–271, https://doi.org/10.1016/j.cellsig.2015.12.011.

[62] J.N. Cobley, G.K. Sakellariou, H. Husi, B. McDonagh, Proteomic strategies to unravel age-related redox signalling defects in skeletal muscle, Free Radical Biol. Med. 132 (2019) 24–32, https://doi.org/10.1016/j.freeradbiomed.2018.09.012.

[63] J.N. Cobley, N.V. Margaritelis, J.P. Morton, G.L. Close, M.G. Nikolaidis, J. K. Malone, The basic chemistry of exercise-induced DNA oxidation: oxidative damage, redox signaling, and their interplay, Front. Physiol. 6 (2015) 182, https://doi.org/10.3389/fphys.2015.00182.

[64] N.V. Margaritelis, V. Paschalis, A.A. Theodorou, A. Kyparos, M.G. Nikolaidis, Redox basis of exercise physiology, Redox Biol. 35 (2020), 101499, https://doi.org/10.1016/j.redox.2020.101499.

[65] D.J. Muggeridge, D.R. Crabtree, A. Tuncay, I.L. Megson, G. Davison, J.N. Cobley, Exercise decreases PP2A-specific reversible thiol oxidation in human erythrocytes: implications for redox biomarkers, Free Radical Biol. Med. 182 (2022) 73–78, https://doi.org/10.1016/j.freeradbiomed.2022.02.019.

[6][6] J.S. O'Neill, G. van Ooijen, L.E. Dixon, C. Troein, F. Corellou, F.-Y. Bouget, A. B. Reddy, A.J. Millar, Circadian rhythms persist without transcription in a eukaryote, Nature 469 (2011) 554–558, https://doi.org/10.1038/nature09654.

[67] M. Ralser, M.M. Wamelink, A. Kowald, B. Gerisch, G. Heeren, E.A. Struys, E. Klipp, C. Jakobs, M. Breitenbach, H. Lehrach, S. Krobitsch, Dynamic rerouting of the carbohydrate flux is key to counteracting oxidative stress, J. Biol. 6 (2007) 10, https://doi.org/10.1186/jbiol61.

[68] D. Peralta, A.K. Bronowska, B. Morgan, É. Dóka, K.V. Laer, P. Nagy, F. Gräter, T. P. Dick, A proton relay enhances H2O2 sensitivity of GAPDH to facilitate metabolic adaptation, Nat. Chem. Biol. 11 (2015) 156–163, https://doi.org/10.1038/nchembio.1720.

[69] M.G. Nikolaidis, A.Z. Jamurtas, Blood as a reactive species generator and redox status regulator during exercise, Arch. Biochem. Biophys. 490 (2009) 77–84, https://doi.org/10.1016/j.abb.2009.08.015.

[70] C.E. Paulsen, T.H. Truong, F.J. Garcia, A. Homann, V. Gupta, S.E. Leonard, K. S. Carroll, Peroxide-dependent sulfenylation of the EGFR catalytic site enhances kinase activity, Nat. Chem. Biol. 8 (2012) 57–64, https://doi.org/10.1038/nchembio.736.

[71] D.G. Kirova, K. Judasova, J. Vorhauser, T. Zerjatke, J.K. Leung, I. Glauche, J. Mansfeld, A ROS-dependent mechanism promotes CDK2 phosphorylation to drive progression through S phase, Dev. Cell (2022), https://doi.org/10.1016/j.devcel.2022.06.008.

[72] P. Devant, E. Boršić, E.M. Ngwa, H. Xiao, E.T. Chouchani, J.R. Thiagarajah, I. Hafner-Bratkovič, C.L. Evavold, J.C. Kagan, Gasdermin D pore-forming activity is redox-sensitive, Cell Rep. 42 (2023), 112008, https://doi.org/10.1016/j.celrep.2023.112008.

[73] G. Kustatscher, T. Collins, A.-C. Gingras, T. Guo, H. Hermjakob, T. Ideker, K. S. Lilley, E. Lundberg, E.M. Marcotte, M. Ralser, J. Rappsilber, Understudied proteins: opportunities and challenges for functional proteomics, Nat. Methods 19 (2022) 774–779, https://doi.org/10.1038/s41592-022-01454-x.

[74] J. Cobley, A. Noble, R. Bessell, M. Guille, H. Husi, Reversible thiol oxidation inhibits the mitochondrial ATP synthase in Xenopus laevis oocytes, Antioxidants 9 (2020) 215, https://doi.org/10.3390/antiox9030215.

[75] S.-B. Wang, D.B. Foster, J. Rucker, B. O'Rourke, D.A. Kass, J.E.V. Eyk, Redox regulation of mitochondrial ATP synthase, Circ. Res. 109 (2011) 750–757, https://doi.org/10.1161/circresaha.111.246124.

[76] S.-B. Wang, C.I. Murray, H.S. Chung, J.E.V. Eyk, Redox regulation of mitochondrial ATP synthase, Trends Cardiovasc. Med. 23 (2013) 14–18, https://doi.org/10.1016/j.tcm.2012.08.005.
[77] A. Rodríguez-Nuevo, A. Torres-Sanchez, J.M. Duran, C.D. Guirior, M.A. Martínez-Zamora, E. Böke, Oocytes maintain ROS-free mitochondrial metabolism by suppressing complex I, Nature (2022) 1–6, https://doi.org/10.1038/s41586-022-04979-5.
[78] J.N. Cobley, Mechanisms of mitochondrial ROS production in assisted reproduction: the known, the unknown, and the intriguing, Antioxidants 9 (2020) 933, https://doi.org/10.3390/antiox9100933.
[79] D. Kim, A.E. Herr, Protein immobilization techniques for microfluidic assays, Biomicrofluidics 7 (2013), 041501, https://doi.org/10.1063/1.4816934.
[80] A. Tuncay, A. Noble, M. Guille, J.N. Cobley, RedoxiFluor: a microplate technique to quantify target-specific protein thiol redox state in relative percentage and molar terms, Free Radical Biol. Med. 181 (2022) 118–129, https://doi.org/10.1016/j.freeradbiomed.2022.01.023.
[81] M. Wühr, R.M. Freeman, M. Presler, M.E. Horb, L. Peshkin, S.P. Gygi, M. W. Kirschner, Deep proteomics of the Xenopus laevis egg using an mRNA-derived reference database, Curr. Biol. 24 (2014) 1467–1475, https://doi.org/10.1016/j.cub.2014.05.044.
[82] M.L. Blackman, M. Royzen, J.M. Fox, Tetrazine ligation: fast bioconjugation based on inverse-electron-demand Diels−Alder reactivity, J. Am. Chem. Soc. 130 (2008) 13518–13519, https://doi.org/10.1021/ja8053805.
[83] B.L. Oliveira, Z. Guo, G.J.L. Bernardes, Inverse electron demand Diels–Alder reactions in chemical biology, Chem. Soc. Rev. 46 (2017) 4895–4950, https://doi.org/10.1039/c7cs00184c.
[84] N.J. Day, M.J. Gaffrey, W.-J. Qian, Stoichiometric thiol redox proteomics for quantifying cellular responses to perturbations, Antioxidants 10 (2021) 499, https://doi.org/10.3390/antiox10030499.
[85] X. Li, N.J. Day, S. Feng, M.J. Gaffrey, T.-D. Lin, V.L. Paurus, M.E. Monroe, R. J. Moore, B. Yang, M. Xian, W.-J. Qian, Mass spectrometry-based direct detection of multiple types of protein thiol modifications in pancreatic beta cells under endoplasmic reticulum stress, Redox Biol. 46 (2021), 102111, https://doi.org/10.1016/j.redox.2021.102111.
[86] L.J. Alcock, M.V. Perkins, J.M. Chalker, Chemical methods for mapping cysteine oxidation, Chem. Soc. Rev. 47 (2017) 231–268, https://doi.org/10.1039/c7cs00607a.
[87] Y. Shi, K.S. Carroll, Activity-based sensing for site-specific proteomic analysis of cysteine oxidation, Accounts Chem. Res. 53 (2020) 20–31, https://doi.org/10.1021/acs.accounts.9b00562.
[88] R.B. Ferreira, L. Fu, Y. Jung, J. Yang, K.S. Carroll, Reaction-based fluorogenic probes for detecting protein cysteine oxidation in living cells, Nat. Commun. 13 (2022) 5522, https://doi.org/10.1038/s41467-022-33124-z.
[89] A.V. Peskin, C.C. Winterbourn, Assay of superoxide dismutase activity in a plate assay using WST-1, Free Radical Biol. Med. 103 (2017) 188–191, https://doi.org/10.1016/j.freeradbiomed.2016.12.033.
[90] D. Su, M.J. Gaffrey, J. Guo, K.E. Hatchell, R.K. Chu, T.R.W. Clauss, J.T. Aldrich, S. Wu, S. Purvine, D.G. Camp, R.D. Smith, B.D. Thrall, W.-J. Qian, Proteomic identification and quantification of S-glutathionylation in mouse macrophages using resin-assisted enrichment and isobaric labeling, Free Radical Biol. Med. 67 (2014) 460–470, https://doi.org/10.1016/j.freeradbiomed.2013.12.004.
[91] S. Akter, L. Fu, Y. Jung, M.L. Conte, J.R. Lawson, W.T. Lowther, R. Sun, K. Liu, J. Yang, K.S. Carroll, Chemical proteomics reveals new targets of cysteine sulfinic acid reductase, Nat. Chem. Biol. 14 (2018) 995–1004, https://doi.org/10.1038/s41589-018-0116-2.
[92] Y. Hao, T.F. Langford, S.J. Moon, K.A. Eller, H.D. Sikes, Screening compound libraries for H2O2-mediated cancer therapeutics using a peroxiredoxin-based sensor, Cell Chem Biol (2021), https://doi.org/10.1016/j.chembiol.2021.09.003.
[93] B. Morgan, K.V. Laer, T.N.E. Owusu, D. Ezeriņa, D. Pastor-Flores, P.S. Amponsah, A. Tursch, T.P. Dick, Real-time monitoring of basal H2O2 levels with peroxiredoxin-based probes, Nat. Chem. Biol. 12 (2016) 437–443, https://doi.org/10.1038/nchembio.2067.
[94] C.A. Bellissimo, L.J. Delfinis, M.C. Hughes, P.C. Turnbull, S. Gandhi, S. N. DiBenedetto, F.A. Rahman, P. Tadi, C.A. Amaral, A. Dehghani, J. Cobley, J. Quadrilatero, U. Schlattner, C.G.R. Perry, Mitochondrial Creatine Sensitivity Is Lost in the D2.Mdx Model of Duchenne Muscular Dystrophy and Rescued by the Mitochondrial-Enhancing Compound Olesoxime, Am J Physiol-Cell Ph, 2023, https://doi.org/10.1152/ajpcell.00377.2022.
[95] L. Pillai-Kastoori, A.R. Schutz-Geschwender, J.A. Harford, A systematic approach to quantitative Western blot analysis, Anal. Biochem. 593 (2020), 113608, https://doi.org/10.1016/j.ab.2020.113608.
[96] M.J. MacCoss, J.A. Alfaro, D.A. Faivre, C.C. Wu, M. Wanunu, N. Slavov, Sampling the proteome by emerging single-molecule and mass spectrometry methods, Nat. Methods 20 (2023) 339–346, https://doi.org/10.1038/s41592-023-01802-5.
[97] N. Slavov, Unpicking the proteome in single cells, Science 367 (2020) 512–513, https://doi.org/10.1126/science.aaz6695.
[98] L. Gatto, R. Aebersold, J. Cox, V. Demichev, J. Derks, E. Emmott, A.M. Franks, A. R. Ivanov, R.T. Kelly, L. Khoury, A. Leduc, M.J. MacCoss, P. Nemes, D. H. Perlman, A.A. Petelski, C.M. Rose, E.M. Schoof, J.V. Eyk, C. Vanderaa, J. R. Yates, N. Slavov, Initial recommendations for performing, benchmarking and reporting single-cell proteomics experiments, Nat. Methods (2023) 1–12, https://doi.org/10.1038/s41592-023-01785-3.
[99] A.I. Nesvizhskii, R. Aebersold, Interpretation of shotgun proteomic data, Mol. Cell. Proteomics 4 (2005) 1419–1440, https://doi.org/10.1074/mcp.r500012-mcp200.
[100] R. Aebersold, M. Mann, Mass spectrometry-based proteomics, Nature 422 (2003) 198–207, https://doi.org/10.1038/nature01511.
[101] R. Aebersold, M. Mann, Mass-spectrometric exploration of proteome structure and function, Nature 537 (2016) 347–355, https://doi.org/10.1038/nature19949.
[102] W. Timp, G. Timp, Beyond mass spectrometry, the next step in proteomics, Sci. Adv. 6 (2020), eaax8978, https://doi.org/10.1126/sciadv.aax8978.
[103] J.A. Alfaro, P. Bohländer, M. Dai, M. Filius, C.J. Howard, X.F. van Kooten, S. Ohayon, A. Pomorski, S. Schmid, A. Aksimentiev, E.V. Anslyn, G. Bedran, C. Cao, M. Chinappi, E. Coyaud, C. Dekker, G. Dittmar, N. Drachman, R. Eelkema, D. Goodlett, S. Hentz, U. Kalathiya, N.L. Kelleher, R.T. Kelly, Z. Kelman, S.H. Kim, B. Kuster, D. Rodriguez-Larrea, S. Lindsay, G. Maglia, E.M. Marcotte, J.P. Marino, C. Masselon, M. Mayer, P. Samaras, K. Sarthak, L. Sepiashvili, D. Stein, M. Wanunu, M. Wilhelm, P. Yin, A. Meller, C. Joo, The emerging landscape of single-molecule protein sequencing technologies, Nat. Methods 18 (2021) 604–617, https://doi.org/10.1038/s41592-021-01143-1.
[104] J.I. MacDonald, H.K. Munch, T. Moore, M.B. Francis, One-step site-specific modification of native proteins with 2-pyridinecarboxyaldehydes, Nat. Chem. Biol. 11 (2015) 326–331, https://doi.org/10.1038/nchembio.1792.
[105] A.J. Rabalski, A.R. Bogdan, A. Baranczak, Evaluation of chemically-cleavable linkers for quantitative mapping of small molecule-cysteinome reactivity, ACS Chem. Biol. 14 (2019) 1940–1950, https://doi.org/10.1021/acschembio.9b00424.
[106] A.J. Hughes, A.E. Herr, Microfluidic western blotting, Proc. Natl. Acad. Sci. USA 109 (2012) 21450–21455, https://doi.org/10.1073/pnas.1207754110.
[107] T.A. Duncombe, A.M. Tentori, A.E. Herr, Microfluidics: reframing biological enquiry, Nat. Rev. Mol. Cell Biol. 16 (2015) 554–567, https://doi.org/10.1038/nrm4041.
[108] A.J. Hughes, D.P. Spelke, Z. Xu, C.-C. Kang, D.V. Schaffer, A.E. Herr, Single-cell western blotting, Nat. Methods 11 (2014) 749–755, https://doi.org/10.1038/nmeth.2992.